THESIS

CONTEXTUALIZING SOUTHWEST US PRECIPITATION IN PAST AND FUTURE MEAN CLIMATES WITH MARINE HEATWAVES

Submitted by

Olivia E. Lee

Department of Atmospheric Science

In partial fulfillment of the requirements

For the Degree of Master of Science

Colorado State University

Fort Collins, Colorado

Spring 2026

Master's Committee:

Advisor: Maria Rugenstein

Jeremy Rugenstein
Jim Hurrell

ABSTRACT

CONTEXTUALIZING SOUTHWEST US PRECIPITATION IN PAST AND FUTURE MEAN CLIMATES WITH MARINE HEATWAVES

As the Southwest U.S. (SWUS) grapples with continued drought and increased water scarcity, paleoclimate analyses suggest the SWUS was wetter during past warm climates such as the Pliocene. One hypothesis for a wetter SWUS in the Pliocene is that localized warming of the California (CA) margin sea surface temperature (SST) enhanced the North American Monsoon. Marine heatwaves (MHWs) in the eastern Pacific have been suggested as an analog for this mechanism in past and future mean climates. However, the differing timescales complicate this analog: paleoclimate proxies average over thousands of years and represent an equilibrated climate, whereas MHWs are short-lived extreme events. Using millennial-long climate simulations, we test whether the drivers of SWUS precipitation during MHWs are comparable to those governing long-term climate change. Under increased CO_2 forcing, we find no model consensus on the response of equilibrated SWUS precipitation to CA margin warming. In contrast, models agree on an increase in SWUS precipitation when CA margin SST is warmer during MHWs. We use constructed circulation analogs to decompose these responses into the dynamic and thermodynamic contributions. The circulation anomaly during both MHWs and in equilibrium climates enhances SWUS precipitation but through different processes. The thermodynamic response to mean state warming drives strong drying in the SWUS that offsets dynamic wetting, whereas the thermodynamic response to MHWs is negligible. Our findings have different implications for the Pliocene and future mean climates and highlight an important caveat in contextualizing past and future mean climate states with extreme events.

ACKNOWLEDGEMENTS

I would like to thank my advisor, Maria Rugenstein, as well as my co-authors, Jeremy Rugenstein and Senne Van Loon, for providing their mentorship and expertise. Thank you to Jim Hurrell and Jeremy Rugenstein for serving on my committee. Lastly, thank you to my family and friends for endlessly supporting me and encouraging me to pursue my passions.

TABLE OF CONTENTS

LIST OF FIGURES

Chapter 1

Introduction

The Southwest United States (SWUS) is a highly populated region characterized by a semiarid and water sensitive climate. Increased water scarcity due to continuing drought and increasing population growth underscores the importance of understanding the drivers of precipitation in the SWUS. The SWUS is located in a hydroclimatic transition zone between a winter-dominated precipitation regime on the west coast and a summer-dominated regime to the south. Annual precipitation in the SWUS ranges from 127 mm to 500 mm (Figure 1.1), with some regions receiving up to half of their annual precipitation in the summer (Figure 1.2) [1].

A major source of summertime precipitation is the North American Monsoon (NAM), which initiates in western Mexico along the Sierra Madre Occidental in June and migrates northward to New Mexico and Arizona by August. Located at the northward periphery of the NAM region (Figure 1.2), SWUS precipitation variability in the summer is influenced by the NAM. Summertime precipitation in the SWUS is also modulated by patterns of sea surface temperature (SST) [2, 3, 4, 5, 6] and the strength and location of the North Pacific (NPSH) and North Atlantic (NASH) subtropical highs [7, 8]. Wintertime precipitation is driven by extratropical cyclones that bring rain to the lowlands and snow to the mountainous regions. Wintertime precipitation is modulated by modes of Pacific climate variability, such as the El Niño-Southern Oscillation (ENSO) and the Pacific Decadal Oscillation (PDO) [9, 10], and atmospheric modes of variability, such as the east Pacific dipole and the Pacific-North American pattern [11]. The superposition of different modes of variability drives wintertime precipitation variability in the SWUS.

Current observations record a drying trend in the SWUS over the last several decades (Figure 1.3), but future projections of summer SWUS precipitation remain unconstrained (Figure 1.4, top). Several studies on end-of-century projections suggest a drying of SWUS summer precipitation [12, 13, 14, 15], while others instead argue for increased summer precipitation by 2100 [16]. As for future projections of the NAM, several studies assert a seasonal shift of monsoon precipitation

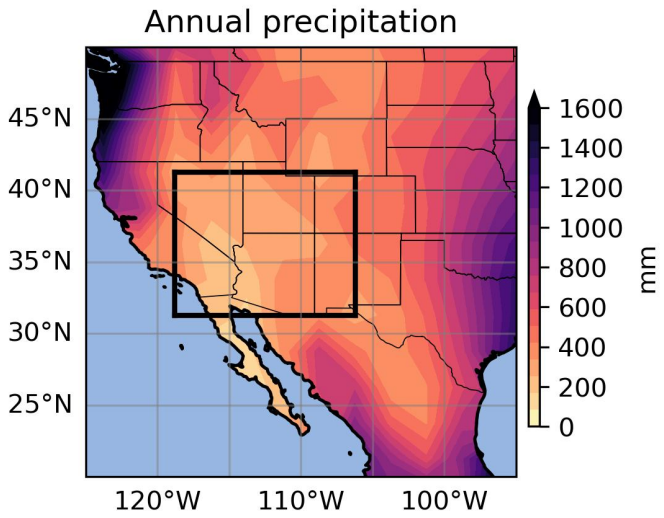

Figure 1.1: Annual mean precipitation in the western US from January 1979 to December 2024. Precipitation obtained from the Global Precipitation Climatology Project (GPCP).

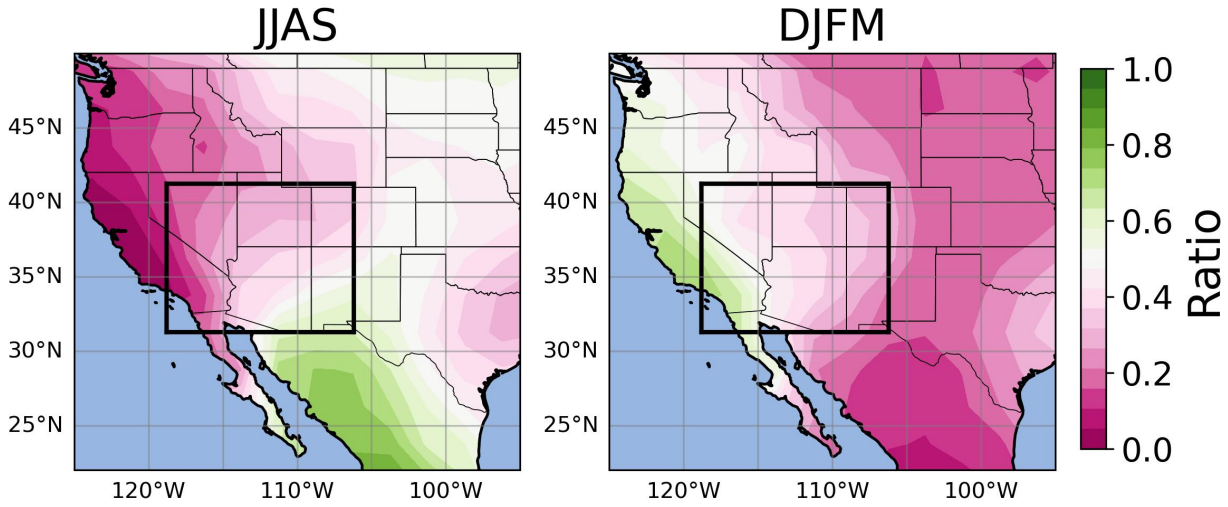

Figure 1.2: Ratio of annual SWUS precipitation that falls in summer (left) and winter (right). Precipitation obtained from the Global Precipitation Climatology Project (GPCP).

from early to late summer [17, 18, 19] and other studies contend an overall weakening of the NAM due to SST warming patterns and increased atmospheric stability [4, 20].

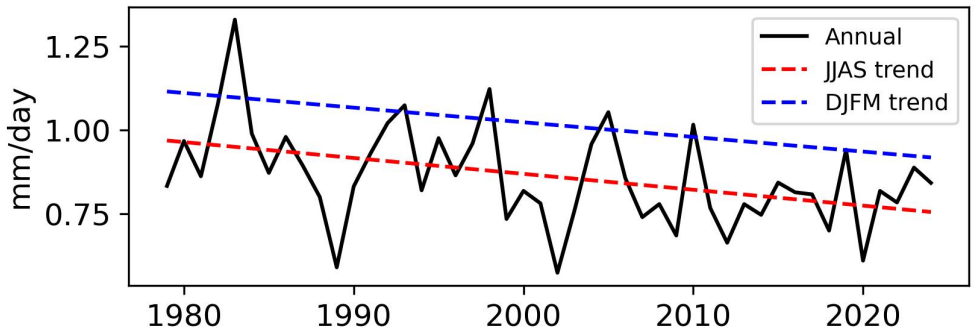

Figure 1.3: Annual mean Southwest US precipitation (black) and trends of summer (red) and winter (blue) precipitation from 1979 to 2024. Precipitation obtained from the Global Precipitation Climatology Project (GPCP).

Similar uncertainty characterizes future projections of wintertime precipitation (Figure 1.4, bottom). Jones et al. (2016) show that CMIP5 models do not agree on the sign of projected changes in wintertime precipitation in the SWUS, whereas Grise (2022) shows that the CMIP6 multimodel mean projects an increase in SWUS wintertime precipitation due to an eastward extension of the subtropical jet stream, which drives enhanced storm track-driven rainfall.

Owing to the uncertainty of SWUS precipitation projections, researchers have frequently looked to past climates to provide insight into future hydroclimates. Such analogs have long been used to aid our understanding of the potential evolution of the climate system, but recent work has called for a more thorough and intentional application of analog frameworks. Oldeman et al. (2025a) distinguish among four types of analogs–forcing, response, process, and rate of change–and argue that explicitly distinguishing the type of analog investigated in a study clarifies both the implications and limitations.

One period that is often suggested as an analog for the current and near-future climate is the mid-Pliocene Warm Period (MPWP) [21, 22, 23]. The MPWP is characterized by a CO_2 concentration of approximately 400 ppm and a global mean surface temperature approximately 4°C

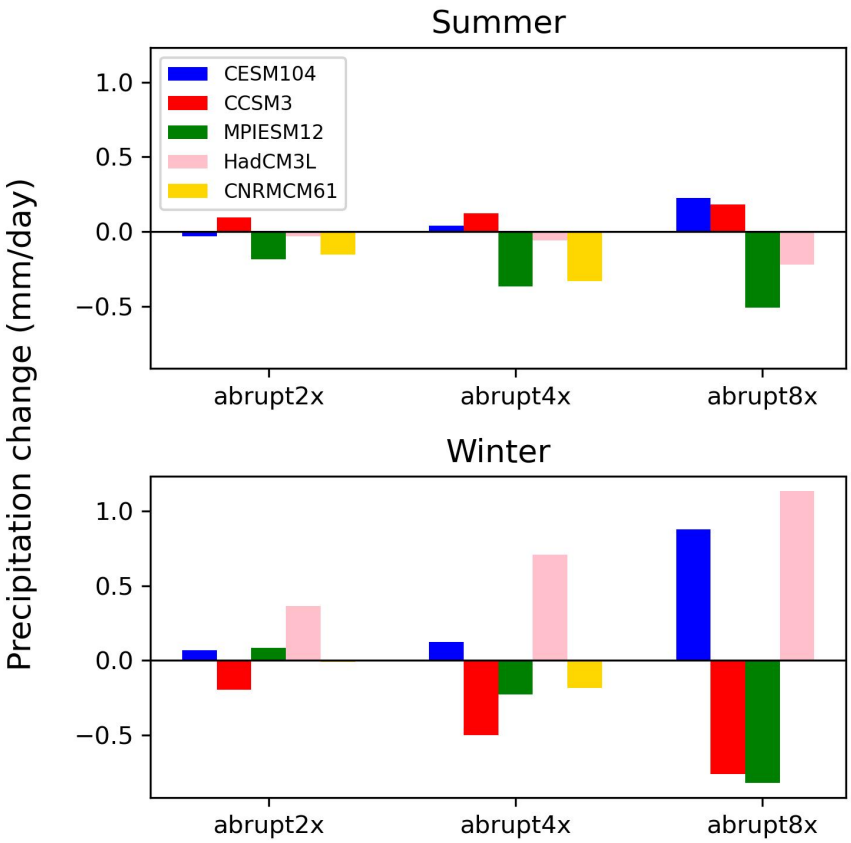

Figure 1.4: Change in Southwest US equilibrium mean summer (top) and winter (bottom) precipitation, relative to the preindustrial control experiment for each model.

warmer than preindustrial [24]. Because of similarities in climate forcings such as CO_2, continental configuration, and large-scale topography, the MPWP constitutes a *forcing* analog, although it is rarely explicitly stated as such.

Despite similarities in climate forcings, proxy data indicate the presence of lakes and expanded forest ecosystems across the SWUS during the MPWP, suggesting that the SWUS hydroclimate was much wetter than today [25, 26, 27]. One hypothesis attributes the wetter SWUS climate during the MPWP to El Niño-like tropical Pacific SST that drives wintertime teleconnections in the SWUS which resemble modern El Niño events [28, 29]. Others propose a role for warmer SST in the northeast Pacific in driving an expanded and enhanced NAM circulation, resulting in more summertime precipitation [30, 31]. Reconstructions of MPWP SST indicate that the region of upwelling along the CA margin was up to 9°C warmer than modern day [32, 33]. In this thesis, we explore the latter hypothesis and therefore focus on summertime precipitation changes.

The mismatch between proxy-inferred pluvial conditions and future-projected aridity implies that the processes governing SWUS precipitation differ between the two climates. This discrepancy motivates a use of analog types other than forcing. Some studies have noted that extreme events share key features with equilibrated climates (e.g., warmer SST, reduced soil moisture, elevated land temperature) [34, 35, 36], suggesting that extreme events can serve as *response* and *process* analogs for mean climates. Bhattacharya et al. (2022) link the 2014 northeast Pacific marine heatwave (MHW) to enhanced NAM precipitation, and propose this modern day relationship as an analog for the NAM during the MPWP. MHWs are discrete periods of enhanced SST relative to the mean local ocean temperature. Past work has sought to understand drivers and biological impacts of individual MHWs [37, 38, 39] and how MHWs will change in a warmer climate [40, 41, 42], but the impacts of MHWs on the SWUS hydroclimate are not well known. Because the eastern Pacific is projected to warm with higher CO_2 forcing, this analog raises the intriguing possibility that MHWs could inform future as well as past changes in SWUS precipitation.

However, proxy data typically averages over thousands of years, thereby reflecting an equilibrated mean climate, whereas MHWs are short-lived extreme events within an equilibrated or

slowly changing climate. Recent research distinguishes between transient and equilibrated hydroclimate responses associated with regional atmospheric circulation changes [43]. Because of this distinction in timescales, we hypothesize that the mechanisms linking warm CA margin SST to SWUS precipitation differs between an equilibrated mean state and MHWs.

In this paper, we investigate the relationship between anomalously warm CA margin SST and SWUS summertime precipitation in two contexts. We first assess the precipitation response to warm, equilibrium CA margin SST driven by enhanced CO_2 forcing, and second to warm CA margin SST during short MHWs. We decompose these precipitation responses into a dynamic and thermodynamic component with a novel application of constructed circulation analogs (CCA). We find that, within a given mean climate, warm extreme CA margin SST is associated with a wetter SWUS. However, this positive relationship does not hold as the CA margin warms across equilibrium climates. That is, models disagree on whether greater CA margin SST due to mean state warming results in an increase or decrease in SWUS precipitation. In both cases, the low-level circulation increases precipitation but through different dynamical mechanisms. We attribute the discrepancy in the total SWUS precipitation response to differences in thermodynamic-induced precipitation changes. Our finding suggests that MHWs may not serve as reliable response or process analogs for equilibrium mean changes in SWUS precipitation.

Chapter 2

Materials and Methods

2.1 Climate Models and Regions

We use LongRunMIP, a model intercomparison composed of millennial-length simulations from coupled general circulation models [44]. The utility of LongRunMIP is twofold. First, because LongRunMIP simulations are typically run for at least 1000 years after an idealized abrupt CO_2 step forcing, we are able to analyze precipitation after the climate system equilibrates to the CO_2 forcing. Second, millennial-long climate simulations allow for a large sample size of extreme events. Because the sample size of observed extreme events is much smaller due to the limited observational record, we opt for a modeling framework to increase the robustness of our results. In this analysis, the preindustrial control, abrupt2x, abrupt4x, and abrupt8x experiments from CESM1.0.4 [45, 46, 47], CCSM3 [48, 49], MPI-ESM-1.2 [50, 51], HadCM3L [52, 53], and CNRM-CM6-1 [54] are used, with the exception of CNRM-CM6-1 for which abrupt8x is not available. We utilize monthly precipitation, near-surface air temperature (tas), and sea level pressure (SLP). For each model experiment, we use the first 1000 years of data except for the abrupt2x experiment in CNRM-CM6-1 which has only 750 years available. All experiments are regridded to the same resolution of 2.5° latitude x 2.5° longitude prior to analyzing.

The CA margin and SWUS are defined as the area between 111.25-126.25°W (box shown in Figure 3.2) and 18.75-33.75°N and 103.75-118.75°W and 31.25-41.25°N (box shown in Figure B.1 in Appendix B), respectively. Results are sensitive to the box location and size so we show maps for context. We analyze the June-September (JJAS) summer average because of our interest in how precipitation during MHWs might resemble NAM precipitation in equilibrated climates.

2.2 Equilibrium Mean States

The equilibrium mean for each variable is taken to be the average over the last 200 years of any given model and simulation. Specifically, the equilibrium mean is taken from year 800 to year 1000 after the abrupt forcing except for CNRM-CM6-1 abrupt2x (see above). By year 800, the forced trend in precipitation, SLP, and tas has equilibrated in all models and forcing scenarios. Results from the equilibrium analysis are presented as standardized anomalies (σ) relative to the control: for the equilibrium mean in each abrupt experiment, we remove the control mean and normalize by the control standard deviation. Our goal is to parallel discussions of past mean climates which are often understood relative to our current climate. Additionally, standardizing takes into account differences in variability across models and experiments. Absolute values are shown in Figure B.1 in Appendix B.

2.3 Marine Heatwaves

Despite our primary focus on MHWs, we include marine cold waves (MCWs) in our analysis to highlight the relationship between SWUS precipitation and extreme CA margin SST in general. Note that we do not analyze extreme precipitation, but rather the response of precipitation to extreme CA margin SST. To minimize the effects of the transient adjustment to the CO_2 forcing on our analysis, we remove the first 200 years of each model experiment and detrend the remaining 800 years. We linearly detrend precipitation and SLP and fit a third-order polynomial to detrend tas. We detrend June, July, August, and September separately to obtain monthly anomalies and then compute the JJAS average of the anomalies. MH(C)Ws are then identified as the 90th (10th) percentile of detrended and area-averaged CA margin tas (Figure 2.1). As a result, 80 MHWs and MCWs occur for each model and simulation, with the exception of the abrupt2x experiment of CNRM-CM6-1 which has 55. Our results do not qualitatively change for other definitions of MHW.

We use a composite analysis to assess the spatial pattern of precipitation and SLP during MHWs. To compute the composite, we average precipitation and SLP across all summers charac-

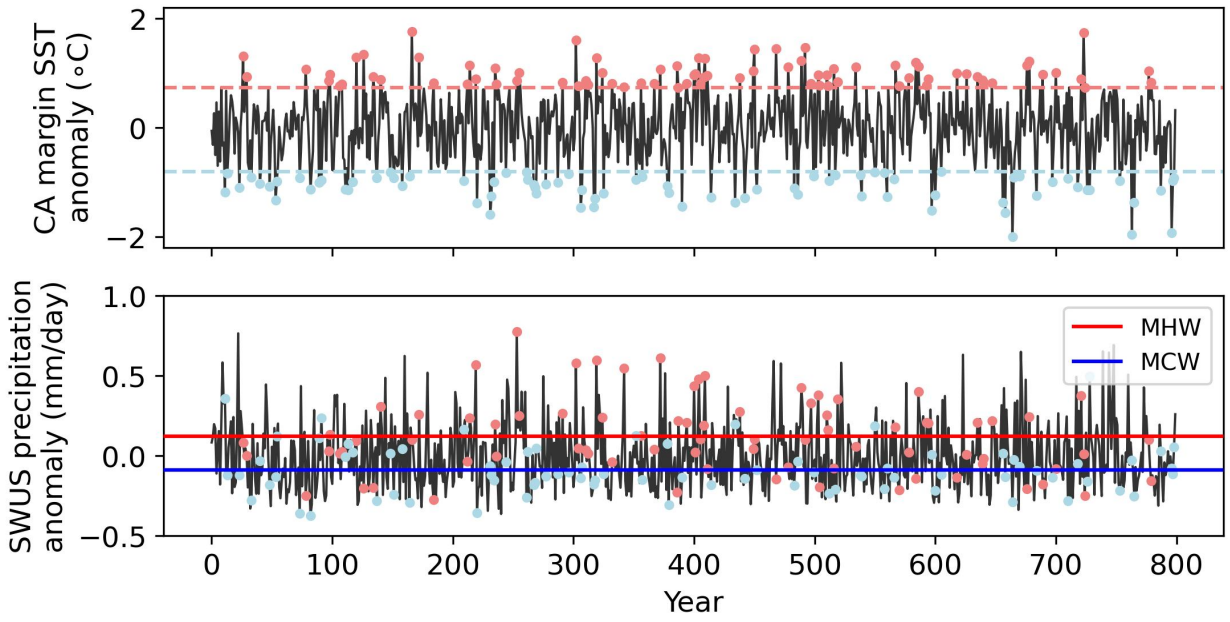

Figure 2.1: MPI-ESM-1.2 abrupt2x California margin sea surface temperature anomaly (top). Light red and blue dashed lines show the 90th and 10th percentile of California margin sea surface temperature, respectively. Light red (blue) markers indicate summers exceeding the 90th (10th) percentile, which are defined as marine heat (cold) wave events. MPI-ESM-1.2 abrupt2x Southwest US precipitation anomaly (bottom). Light red (blue) markers are the same indices as above, indicating marine heat (cold) wave events. The red and blue horizontal lines indicate the composite mean Southwest US precipitation during marine heatwaves and marine cold waves, respectively.

terized by a MHW. Because we are interested in precipitation during MHWs in different mean climates, we present our MHW results as standardized anomalies (σ) relative to each experiment rather than the control. For example, we composite the mean precipitation during MHWs in abrupt4x, remove the abrupt4x mean (which is zero because we detrended), and normalize by the abrupt4x standard deviation. This interpretation is analogous to analyzing observed MHWs in our current climate.

2.4 Impact of ENSO on Marine Heatwaves

Our analysis focuses on the linkage between SST and precipitation in the summer, and ENSO teleconnections are generally stronger in winter than summer. We found that summertime CA margin SST has more power on decadal rather than interannual timescales, indicating a greater influence of lower frequency climate variability such as the PDO on CA margin MHWs than ENSO [55]. Regressing ENSO out of the CA margin SST does not greatly alter the power at the interannual timescale in most models (Figure 2.2). Additionally, a weak relationship exists between ENSO and NAM precipitation [30, 3]. Hence, for the below analysis, we keep the entire signal including a potential subtle ENSO signal.

2.5 Constructed Circulation Analogs

We employ LongRunMIP to increase the sample of MHWs and to clearly isolate the equilibrated climate responses from the transient. These simulations do not provide three-dimensional atmospheric fields, precluding the application of a vertically-integrated moisture budget decomposition. Instead, we use the CCA method, which is well-suited for evaluating process analogs because it conditions precipitation responses on specific circulation states. This approach enables an empirical assessment of whether the same dynamic mechanisms operate during MHWs and under equilibrium mean warming.

For a detailed explanation of our CCA method, see Appendix A. The CCA method is typically applied to observations or a combined observation-model framework with the goal of separating

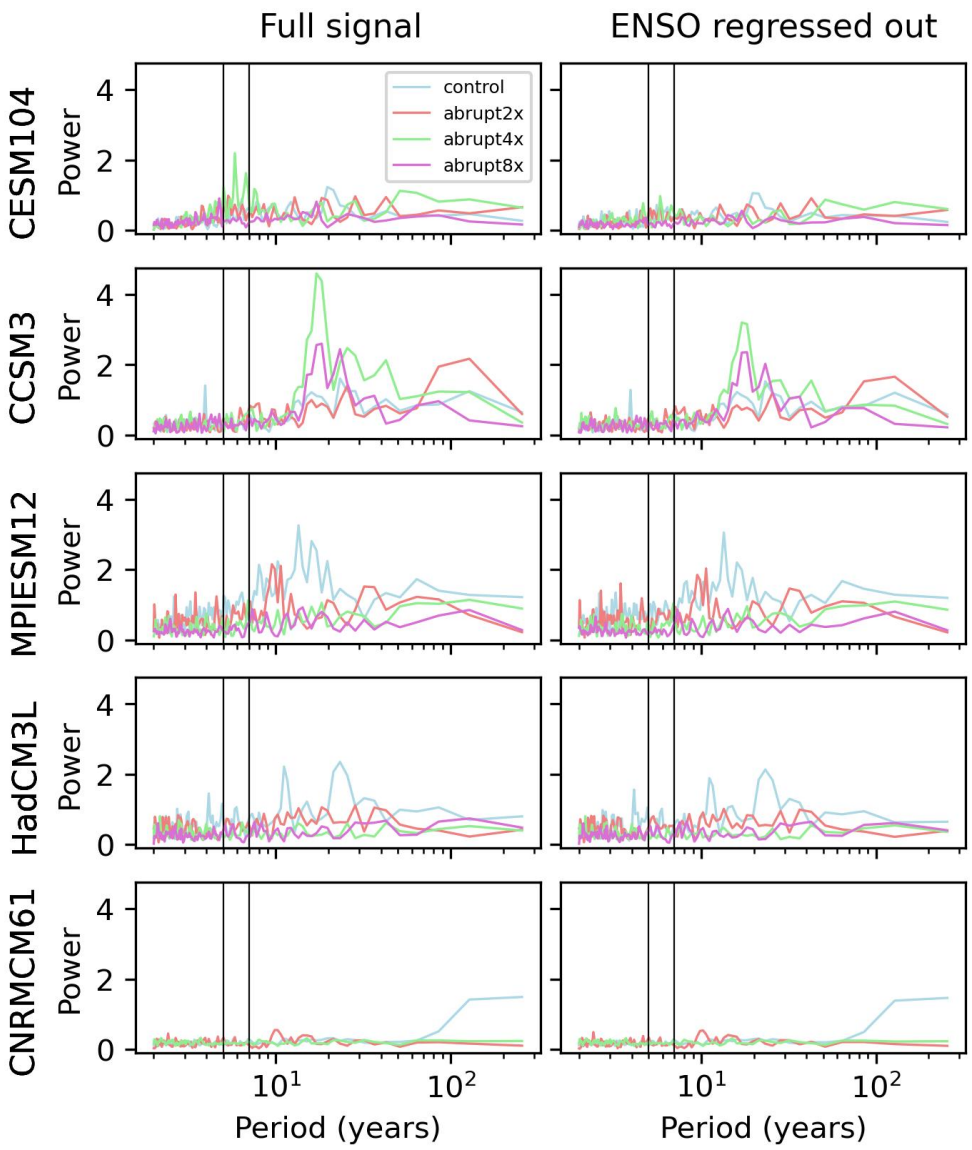

Figure 2.2: Power spectrum of summertime California margin sea surface temperature before (left) and after (right) regressing the Niño3.4 time series out. Vertical lines at 5 and 7 years indicate the the ENSO timescales.

internal circulation variability from internal and forced thermodynamic signals [56, 57]. For our equilibrium analysis, we construct analogs of the forced equilibrium mean SLP anomaly to understand the precipitation associated with the forced circulation change in higher CO_2 climates. The equilibrium mean SLP anomaly represents the difference between the summertime climatological SLP pattern in a climate characterized by a greater CO_2 concentration and the unforced climate. We reconstruct this forced SLP anomaly from a linear combination of control SLP and therefore from internal circulation variability alone, and obtain the associated precipitation pattern. We subtract the dynamic component of SLP and precipitation from the total equilibrium anomaly to get the residual. Because the residual precipitation anomaly is the component of precipitation changes not directly related to SLP changes, we interpret it as the forced thermodynamic component. This assumption is discussed further in section 4.1. The decomposition is performed on absolute SLP and precipitation anomalies in hPa and mm/day, respectively. For visualization purposes, we divide the decomposed precipitation components by the control standard deviation to get the standardized anomalies relative to the control.

We apply a similar method to the MHW case with some key differences. One major difference is that we reconstruct the MHW SLP anomaly from the non-MHW years in each respective abrupt experiment as opposed to the control experiment. This is because we aim to reconstruct the SLP anomaly during an extreme event from the internal atmospheric circulation variability that is characteristic of the climate in which the extreme occurred. Additionally, we reconstruct the MHW SLP anomaly from the non-MHW years because our goal is to isolate the precipitation driven by internal atmospheric variability from the precipitation due to the MHW forcing. As before, we subtract the linearly reconstructed variable maps from the total anomaly to get the thermodynamic residual. Hereafter we refer to the residual as the thermodynamic component. We divide the precipitation components by the respective experiment standard deviation for easier comparison across models and with the equilibrium scenario.

Chapter 3

Southwest US Precipitation Response to California Margin Warming

3.1 Models Disagree on the Precipitation Change Associated with Equilibrium Mean Warming

Prominent features of the control mean summertime precipitation include the NAM region in western Mexico, the low level jet in Great Plains, and the region of dryness in the western US (Figure 3.1a-e). Control summer precipitation coincides with low SLP over the western US and high pressure over the eastern Pacific and western Atlantic. The presence of the North Pacific (NPSH) and North Atlantic (NASH) Subtropical Highs strongly influences precipitation in the central and western US. A westward expansion of the NASH in the summer is associated with an enhanced southerly low level jet and increased precipitation in the Great Plains. In contrast, the eastern flank of NPSH is associated with subsidence and equatorward flow from higher latitudes which promotes SWUS aridity [58, 15]. Therefore, model differences in the location and intensity of the NPSH and NASH contribute to intermodel differences of SWUS precipitation. The simulation of the NAM also contributes to SWUS precipitation variability across models. MPI-ESM-1.2 displays the most widespread monsoon signature with precipitation reaching into southern New Mexico and Arizona while CCSM3 has the weakest NAM with no northward extension into the US. The multimodel mean control precipitation in the SWUS is 1.0 mm/day. MPI-ESM-1.2 and HadCM3L simulate the driest and wettest SWUS at 0.7 mm/day and 1.4 mm/day, respectively.

Increasing CA margin SST with higher CO_2 forcing is a robust response across models (Figure 3.2). We therefore use a range of idealized CO_2 forcing scenarios as a proxy for warming CA margin SST and assess equilibrium mean SWUS precipitation changes across these experiments. The cross-model control mean CA margin temperature is $23.0°$C and the mean equilibrium warming

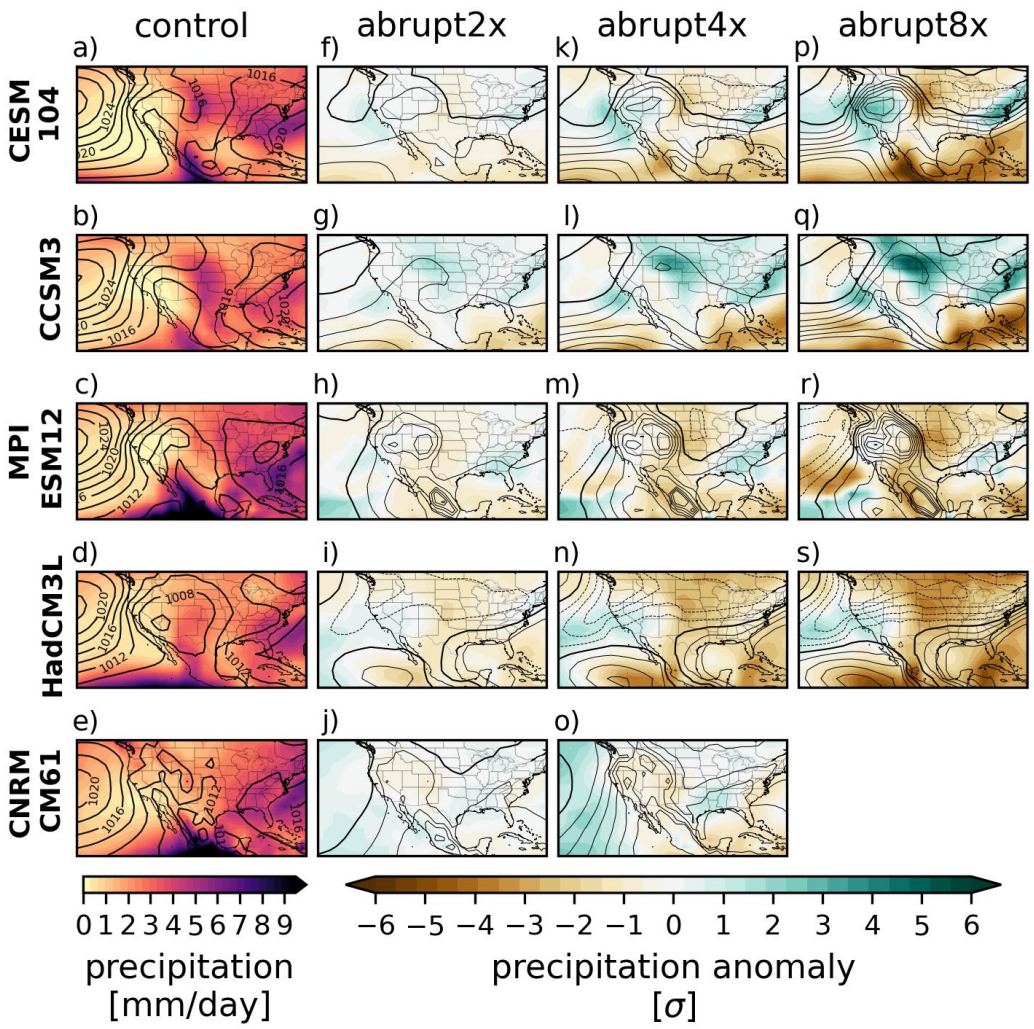

Figure 3.1: Control equilibrium mean summer precipitation (colors) and sea level pressure (black contours, 2 hPa increments) (a-e) and abrupt2x (f-j), abrupt4x (k-o), and abrupt8x (p-s) standardized anomalies of precipitation (colors) and sea level pressure (black contours, 1 standard deviation increments, thick lines represent no change and thin solid and dashed lines represent an increase and decrease in sea level pressure, respectively) with respect to the control.

relative to the control is 2.2, 4.7, and 6.7°C in the abrupt2x, abrupt4x, and abrupt8x simulations, respectively. Across models, the abrupt8x CA margin SST ranges from 4.7°C to 9.3°C and therefore most closely resembles CA margin SST during the Pliocene, even though the CO_2 concentration is much higher and the overall Pacific SST pattern differs from that estimated in the Pliocene [33]. Our experimental design does not aim to replicate the Pliocene. Rather, our goal here is to understand SWUS precipitation that is concurrent with warm CA margin SST, regardless of the specific SST pattern, in idealized equilibrium scenarios.

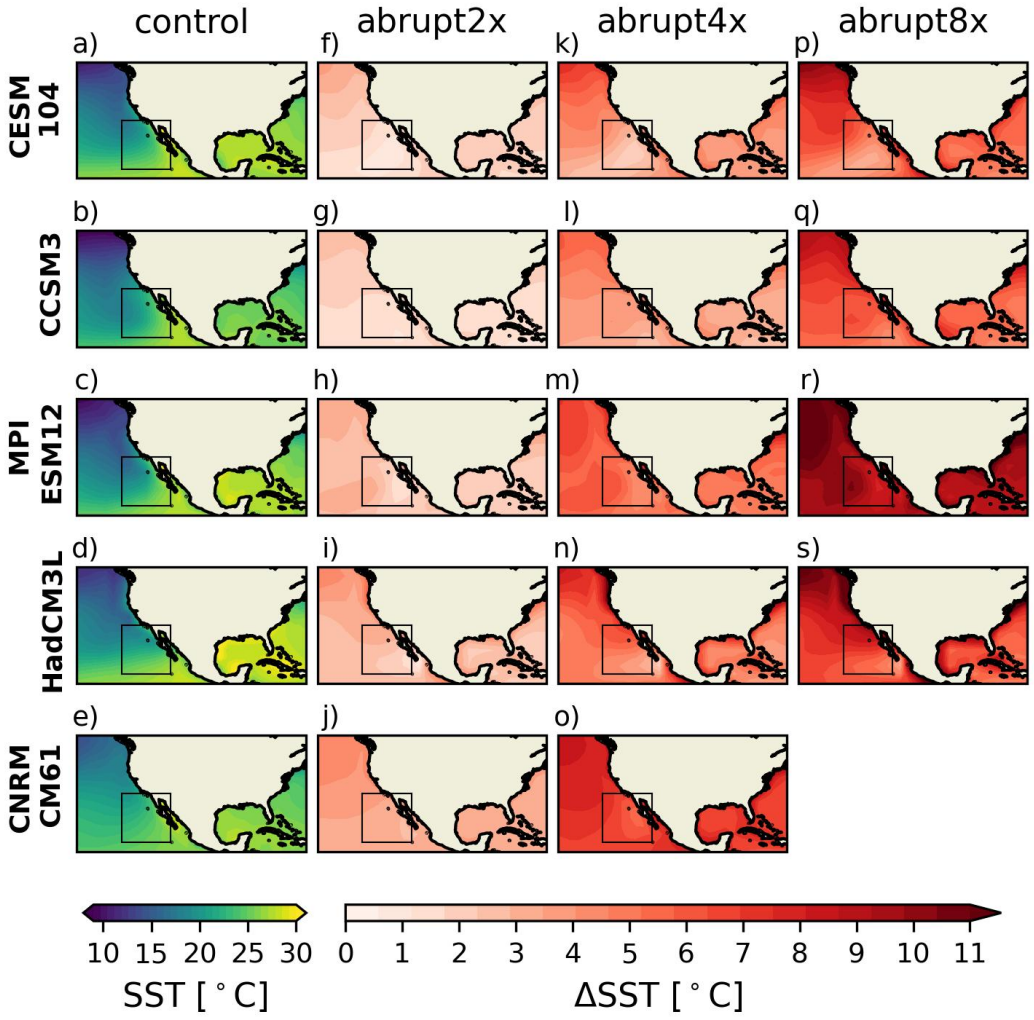

Figure 3.2: Control equilibrium mean summer sea surface temperature (colors) (a-e) and abrupt2x (f-j), abrupt4x (k-o), and abrupt8x (p-s) absolute anomalies of sea surface temperature (colors) with respect to the control

Despite abrupt8x CA margin SST approaching the warmth inferred by Pliocene reconstructions, few models reflect the wetter SWUS suggested by proxies. In warmer equilibrium climates, models generally project drying in regions of high control precipitation including the core NAM region (Figure 3.1f-s). The spatial distribution of precipitation changes is highly model dependent. While HadCM3L and MPI-ESM-1.2 generally indicate widespread drying over the US with enhanced forcing, the change in precipitation in CESM1.0.4 and CCSM3 is more spatially heterogeneous. MPI-ESM-1.2 simulates the driest SWUS in the control, as well as the greatest drying with higher forcing. By abrupt8x, SWUS precipitation is $-2.2\ \sigma$ less than the control in MPI-ESM-1.2 (Figure 3.1r and 4.1a). In contrast, CCSM3 simulates the greatest wetting with a $1.0\ \sigma$ increase in abrupt8x relative to the control (Figure 3.1q and 4.1a). The multimodel mean change in SWUS precipitation in the abrupt8x climate (excludes CNRM-CM-6.1) is $-0.3\ \sigma$. This range highlights the uncertainty of SWUS precipitation projections and exemplifies the caution needed when interpreting multimodel mean SWUS precipitation.

Most models agree on the intensification of the climatological high pressure over the western US due to the thermal expansion of the lower troposphere [59, 60]. HadCM3L instead simulates a zonal decrease in pressure in most of the US (Figure 3.1i, n, s). CESM1.0.4, CCSM3, and HadCM3L precipitation changes in the western US align with the geostrophic flow expected from the SLP anomalies: enhanced precipitation induced by onshore flow. On the other hand, the SWUS dries in MPI-ESM-1.2 and CNRM-CM6-1 despite simulating similar SLP patterns to CESM1.0.4, indicating that changes in surface level circulation are not the sole driver of SWUS precipitation changes in warmer climates (Figure 3.1h, m, r and j, o). The change in precipitation scales with CO_2 forcing in all models, suggesting an important thermodynamic role in SWUS precipitation changes.

3.2 Enhanced Southwest US Precipitation Associated with Extreme Warming

We next assess the relationship between CA margin SST and SWUS precipitation during MCWs and MHWs. Most models indicate a statistically significant positive relationship between extreme CA margin SST and SWUS precipitation with the exception of CCSM3 which has a significant negative relationship (Figure 3.3). The only scenarios that do not indicate a significant relationship at the 0.05 significance level are HadCM3L abrupt4x and abrupt8x. Besides these scenarios, the positive relationship is robust across forcing levels and the strength of the relationship is relatively independent of the degree of the forcing. In other words, within any given mean climate, the response of SWUS precipitation to extreme CA margin SST during MHWs is the same regardless of the CO_2 concentration that characterizes that climate. We obtain similar results when we include all years in the regression rather than just the extremes (Figure 3.3, gray markers).

Across models, the SST pattern during MHWs features localized warming in the CA margin (Figure 3.4) as opposed to the more uniform warming of the eastern Pacific in equilibrium (Figure 3.2). All models except CCSM3 simulate increased precipitation over the SWUS in the composite mean precipitation during MHWs, although with varying spatial patterns across the US (Figure 3.5). In CESM1.0.4, extensive enhanced precipitation coincides with anomalous high pressure over the western US, low level onshore flow in the Northwest, and offshore flow near Baja CA (Figure 3.5a-d). MPI-ESM-1.2 and CNRM-CM6-1 also simulate anomalous high pressure over the western US that coincides with greater precipitation, however the SLP pattern in these models differ from CESM1.0.4 over the ocean. These models simulate a strong negative SLP anomaly over the NPSH region (Figure 3.5i-l and 3.5q-s) which inhibits cool, dry northerly flow over the eastern flank of the NPSH, allowing for the transport of warm, moist air from the tropics into the Gulf of CA [2]. Warm SST in the Gulf of CA has been shown to be a necessary condition for NAM convection [61, 62], suggesting that a wetter SWUS during MHWs is mediated by the NAM. The negative SLP anomaly over the NPSH is also present in CCSM3, however the composite shows

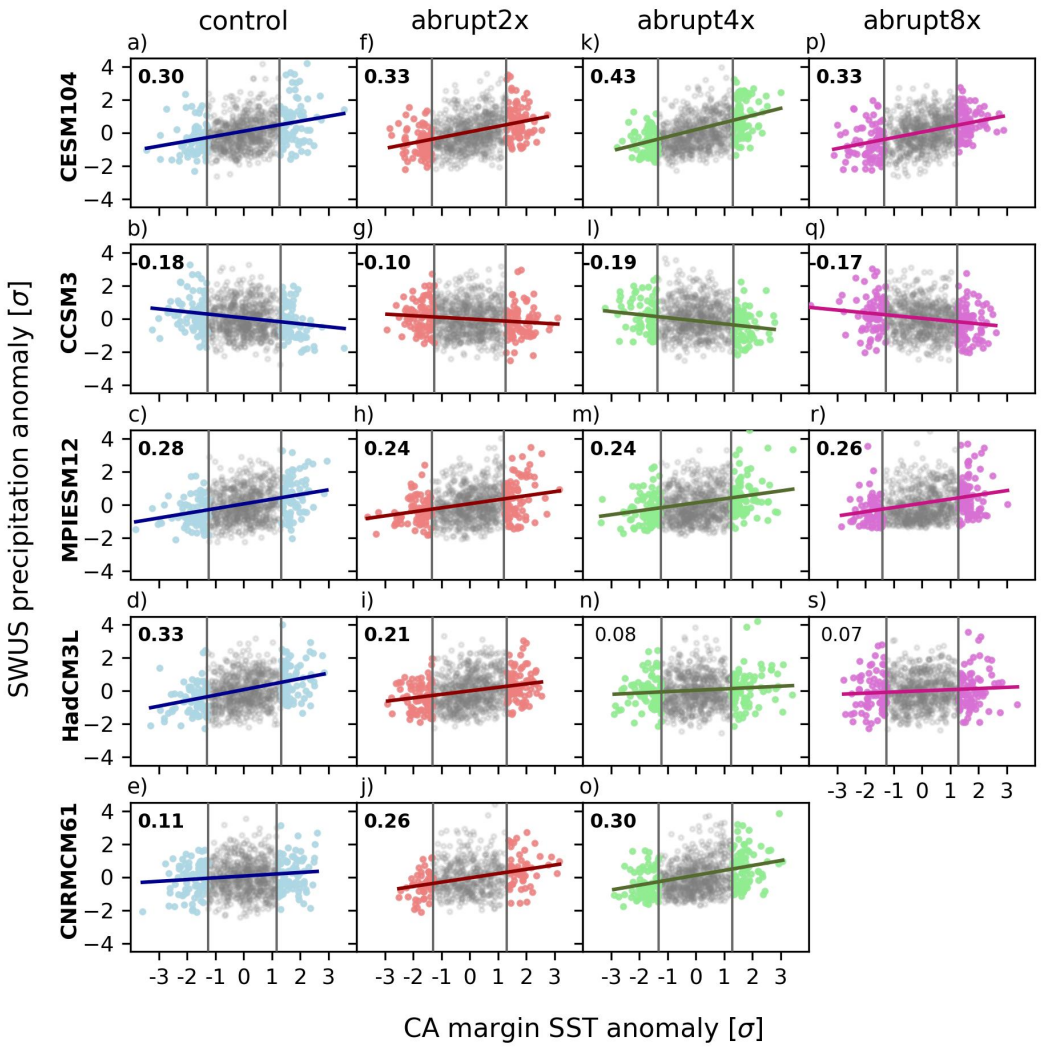

Figure 3.3: California margin sea surface temperature and Southwest US precipitation standardized anomalies during 10th and 90th percentile California margin sea surface temperature summers (colored markers; gray markers show all other summers). The colored solid lines show the linear regression of Southwest US precipitation onto extreme California margin sea surface temperature. The gray solid lines denote the 10th and 90th percentile of California margin sea surface temperature for each experiment. The regression slopes are noted in the upper left of each plot and are bolded if significant at the 0.05 significance level.

wetter conditions south of the Gulf of CA and into central Mexico but drying over the SWUS (Figure 3.5e-h). The pattern of precipitation and SLP anomalies during MHWs is similar across forcing simulations for each model, again suggesting that enhanced CO_2 does not directly affect the mechanism driving precipitation during MHWs.

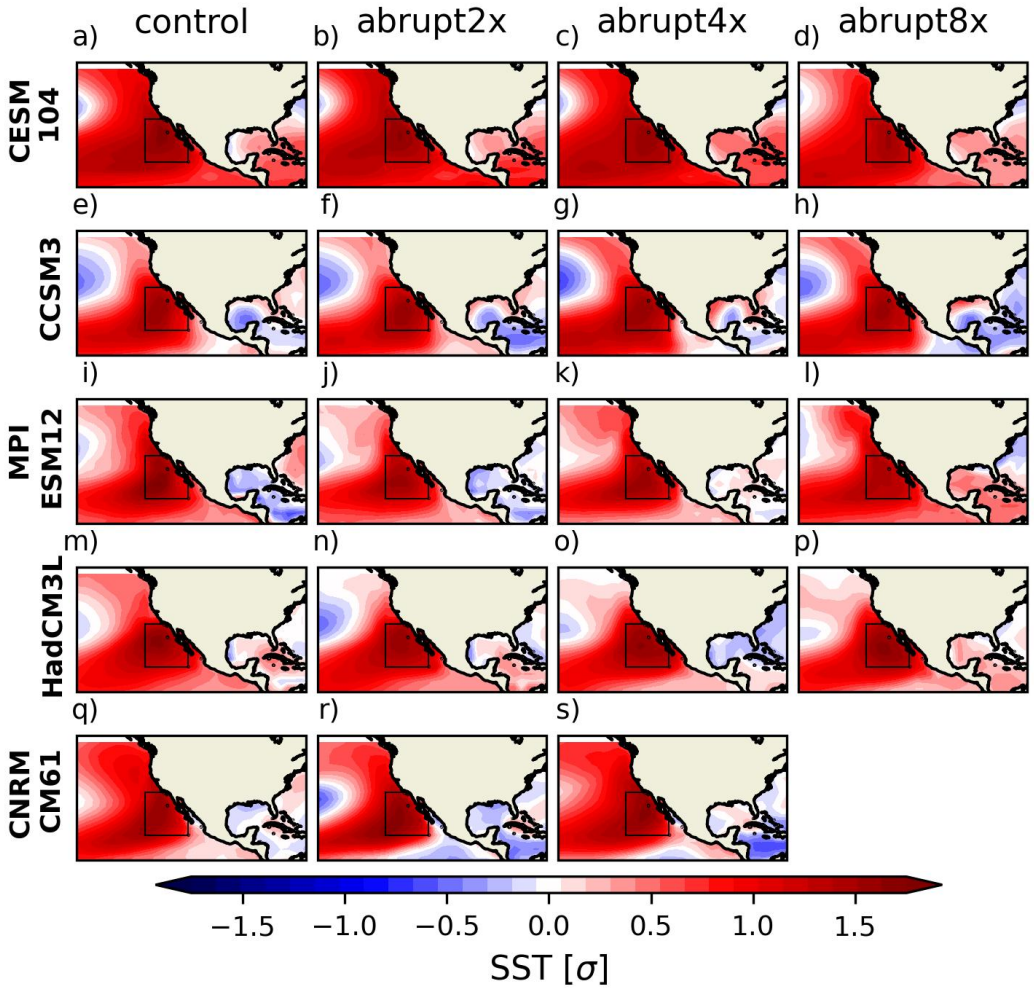

Figure 3.4: Standardized anomaly composites of sea surface temperature during marine heatwaves.

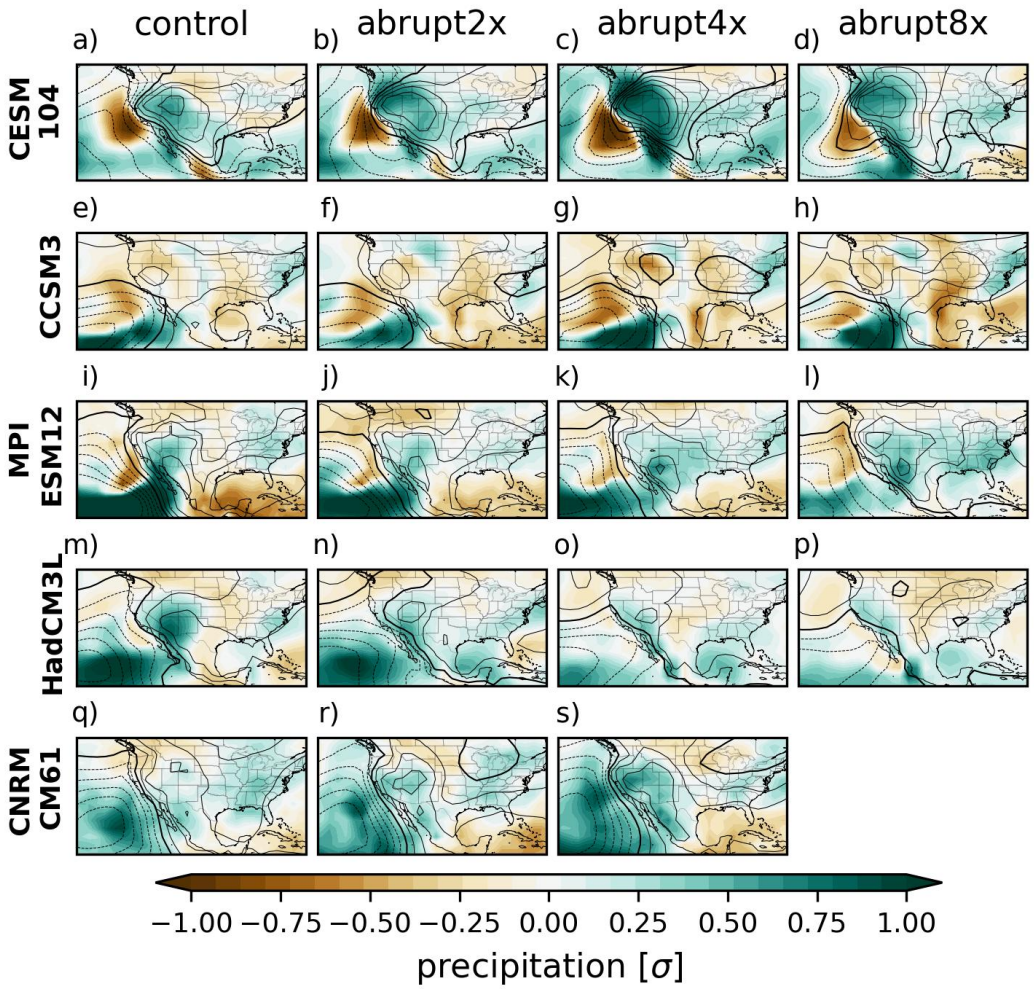

Figure 3.5: Standardized anomaly composites of precipitation (colors) and sea level pressure (black contours, increments of 0.2 standard deviations, thick lines represent no change and thin solid and dashed lines represent an increase and decrease in sea level pressure, respectively) during marine heatwaves.

Chapter 4

Extreme and Equilibrium Mean California Margin Sea Surface Temperature Drive Different Southwest US Precipitation Responses

The response of SWUS precipitation differs when anomalously warm CA margin SST is a signature of mean state warming driven by increased CO_2 versus a temporal anomaly within a given mean climate state. Warmer CA margin SST driven by internal variability increases SWUS precipitation, independent of the CO_2 forcing and robustly across climate models (except CCSM3) (Figure 4.1a, faded lines at each CO_2 level). On the other hand, models disagree on how equilibrium SWUS precipitation responds to CA margin warming driven by increased CO_2 (Figure 4.1a, markers and opaque lines).

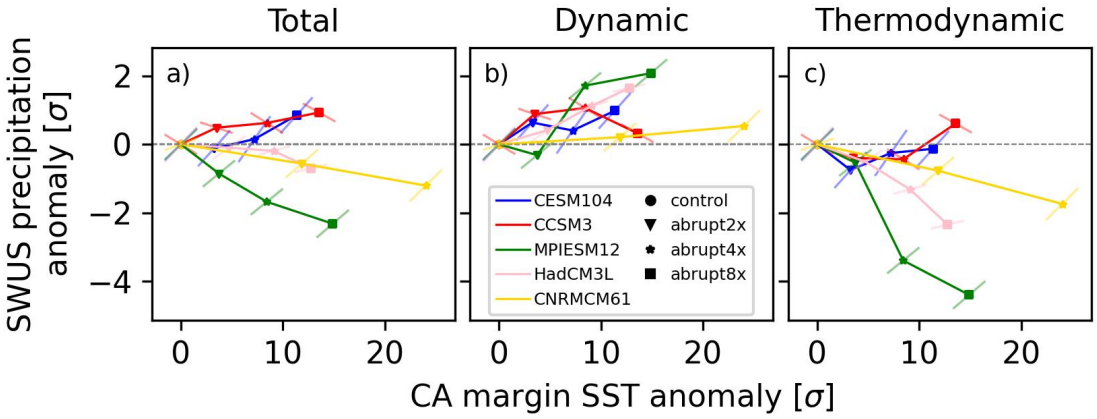

Figure 4.1: Equilibrium mean California margin sea surface temperature standardized anomalies and total (a), circulation-driven (b), and thermodynamic (c) Southwest US precipitation standardized anomalies (solid lines and markers). Faded lines show the regression slope between California margin sea surface temperature and Southwest US precipitation during marine heatwaves at each CO_2 level (from Figure 3.3).

To understand the model spread in SWUS equilibrium responses and the discrepancy in equilibrium and MHW precipitation (Figure 4.1a), we decompose the SWUS precipitation response in

equilibrated climates (Figure 3.1) and during MHWs (Figure 3.5) into the dynamic and thermodynamic components. For concision, we show the results for MPI-ESM-1.2 here (the equilibrium decomposition for all models and experiments is shown in Figures B.2-3 in Appendix B). Because SWUS precipitation during MHWs does not vary appreciably across experiments, we show the decomposition of precipitation during MHWs for just the abrupt4x mean climate (the MHW decomposition for all models and experiments is shown in Figures B.4-5 in Appendix B).

4.1 The Dynamic and Thermodynamic Components of Southwest US Precipitation in Equilibrium Climates Compete

In MPI-ESM-1.2, the low-level circulation anomaly is associated with a wetting of the western US (Fig 4.2d-f). The strengthening high SLP in the western US promotes onshore geostrophic flow and moisture advection from the Pacific. Additionally, the expansion of the ridge drives anomalous midtropospheric easterly flow from the humid Great Plains, enhancing precipitation in the SWUS [63, 13]. While the circulation anomaly increases precipitation in the western US, it inhibits precipitation in the core NAM region in Mexico. The area of high SLP in Mexico implies a suppression of thermal lows that are associated with enhanced NAM precipitation [64, 65]. The precipitation dipole between the SWUS and Mexico indicates that changes in the overall NAM circulation are not the sole driver of circulation-induced precipitation changes in western North America in equilibrium.

The thermodynamic component is characterized by a negative precipitation anomaly in the SWUS (Fig 4.2g-i). Byrne and O'Gorman (2015) show that increased horizontal gradients of temperature and moisture between land and ocean in a warmer climate modulate precipitation responses over land. The land-ocean gradients may limit the effectiveness of warm SST, especially in the Gulf of CA, in saturating near-surface air and generating convection in the NAM region [60, 15]. The weakening of NAM precipitation also results from increased tropospheric stability associated with increased subtropical subsidence and reduced buoyancy [20].

Local land surface changes are also expected to enhance SWUS aridity. The land surface in moisture-limited regimes such as the SWUS is unable to sustain the evaporation needed to meet the rising saturation vapor pressure of the atmosphere, resulting in an increased vapor pressure deficit, which further exacerbates the arid land surface [66, 67]. Changes in soil moisture, incoming radiation, and stomatal effects are also important in determining evapotranspiration in semi-arid regions [68, 69, 70, 71]. Taken together, the thermodynamic component in our analysis may be a result of a combination of local land-atmosphere feedbacks, reduced NAM convection driven by increased atmospheric stability, and differences in the partitioning of moist static energy into latent and sensible heat over ocean and land [72].

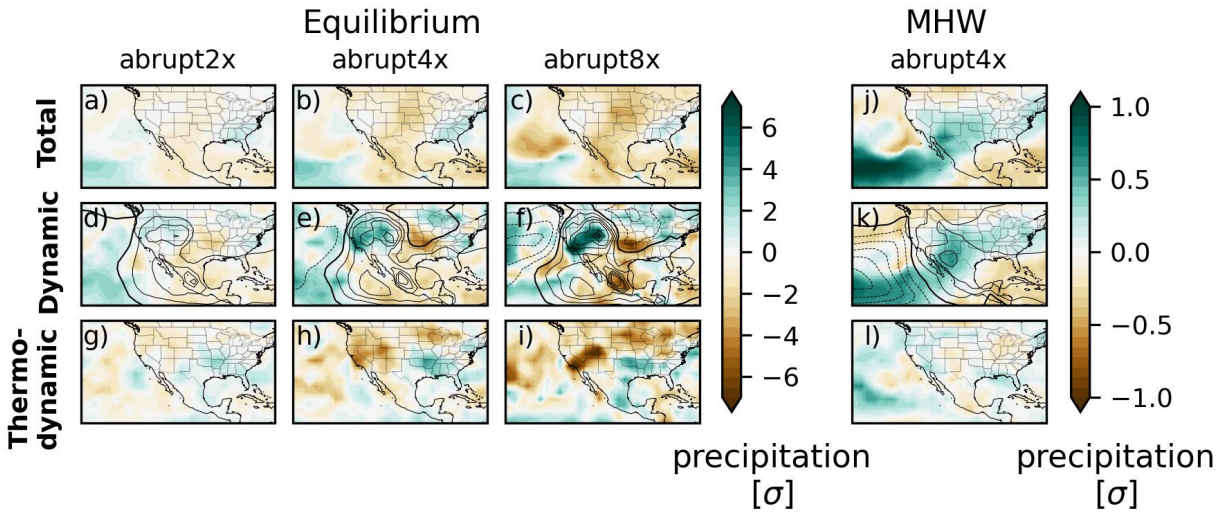

Figure 4.2: The total (a-c), circulation-driven (d-f), and thermodynamic (g-i) equilibrium mean precipitation anomaly (colors) in MPI-ESM-1.2 across experiments. The total (j), circulation-driven (k), and thermodynamic (l) precipitation anomaly (colors) during marine heatwaves in MPI-ESM-1.2 abrupt4x. The black contours show the constructed equilibrium mean (d-f, increments of 1 standard deviation) and marine heatwave (k, increments of 0.2 standard deviations) sea level pressure anomaly. The thick black lines represent no change in sea level pressure while the thin solid and dashed lines represent an increase and decrease in sea level pressure, respectively.

In MPI-ESM-1.2, the thermodynamic drying overcomes the dynamic wetting, resulting in a total dry anomaly in the SWUS (Figure 4.2a-c, same as in Figure 3.1h, m, r). The thermodynamic precipitation component is of the same order of magnitude as the dynamic component

across models, and the equilibrium mean SLP anomaly tends to drive a wetter SWUS while the thermodynamic component dries the SWUS (Figure 4.3a-e). Whether the dynamic or thermodynamic contribution dominates depends on the model (Figure 4.4). In MPI-ESM-1.2, HadCM3L, and CNRM-CM6-1, the drying of the SWUS driven by thermodynamic effects dominates weaker, dynamic-driven wetting (Figure 4.3c-e, 4.4). In CESM1.0.4, dynamic wetting overcomes thermodynamic drying in higher forcing scenarios (Figure 4.3a, 4.4).

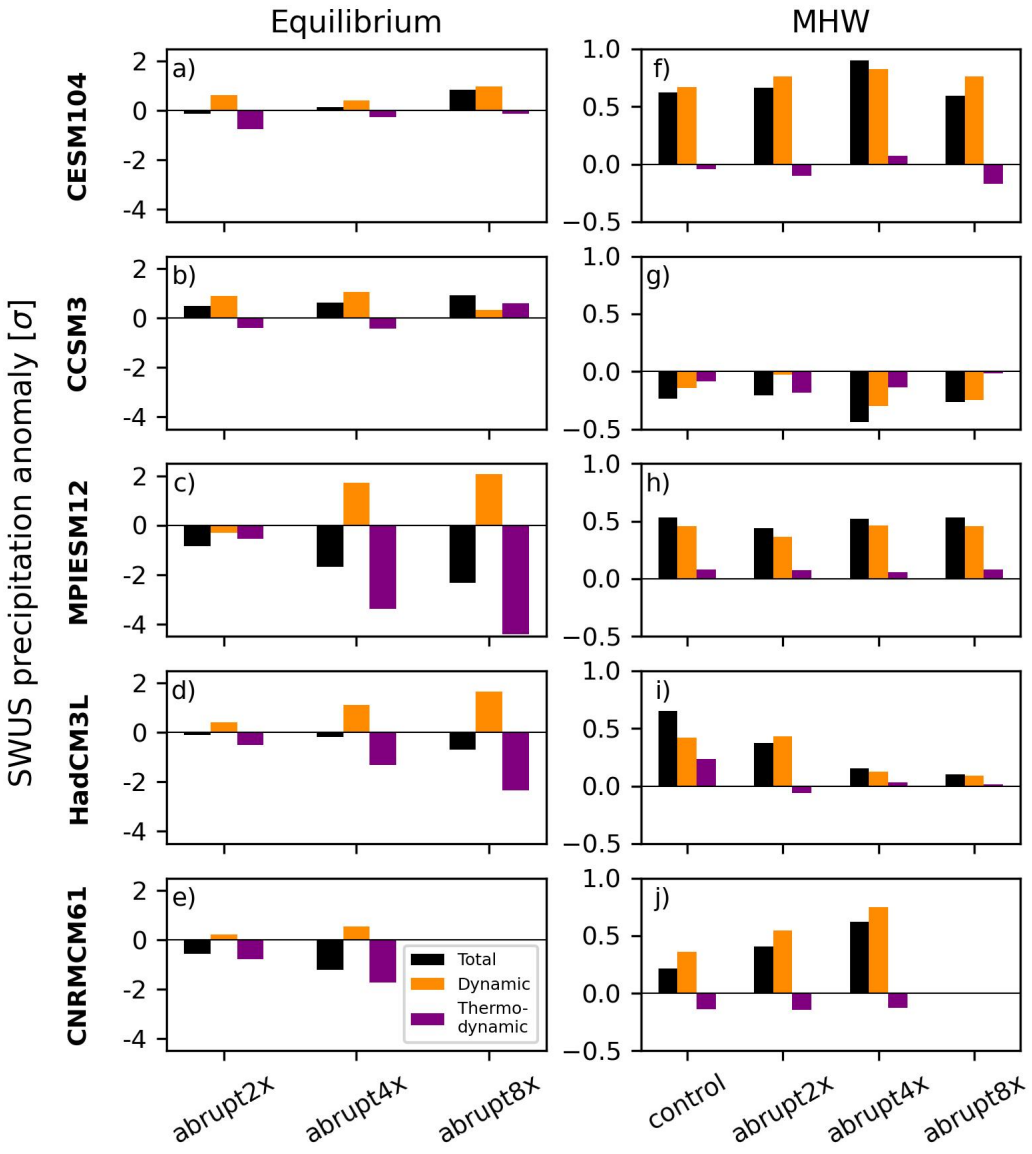

Figure 4.3: The area-averaged total, circulation-driven, and thermodynamic precipitation anomalies in the Southwest US in equilibrium (a-e) and during marine heatwaves (f-j).

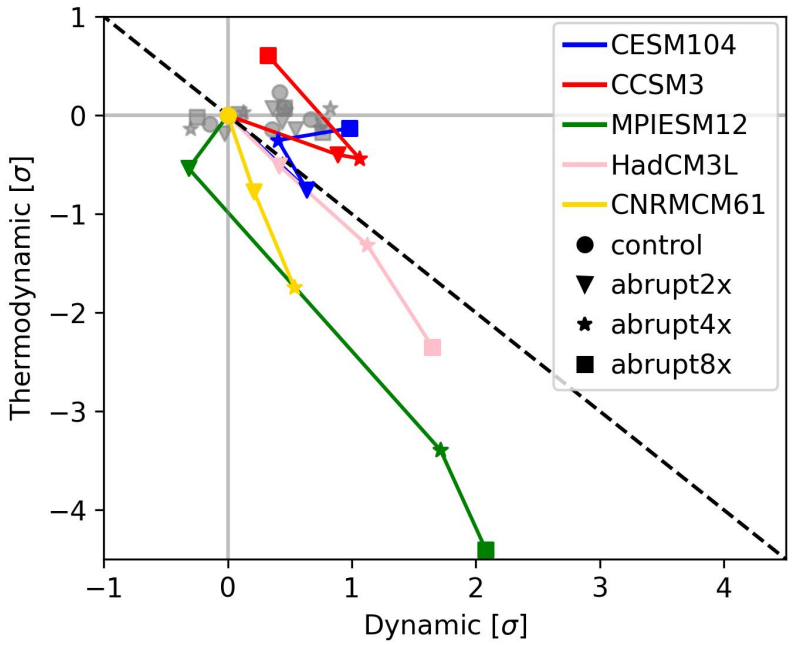

Figure 4.4: Data as in Figure 4.3 but visualized differently. The area-averaged circulation- and thermodynamic-induced precipitation anomalies in the Southwest US across models and experiments. Faded gray markers represent marine heatwaves; colored lines and markers represent equilibrium mean climates. Dashed black line is the 1:1 line between the circulation and the thermodynamic components. Values below (above) the 1:1 line are dominated by the thermodynamic (dynamic) response.

4.2 Southwest US Precipitation During Marine Heatwaves is Predominantly Driven by Dynamics

The total MHW precipitation anomaly in MPI-ESM-1.2 is characterized by a corridor of increased precipitation from the Pacific through the Gulf of CA and enhanced precipitation in the SWUS (Figure 4.2j, same as Figure 3.5k). The negative SLP anomaly over the NPSH region during MHWs allows for anomalous southeasterly flow that enhances moisture in the Gulf of CA (Figure 4.2k). The precipitation reconstruction from internal circulation variability closely resembles the total anomaly, indicating that enhanced SWUS precipitation during MHWs is a primarily dynamic response. The moisture corridor in the Gulf of CA is also present in the thermodynamic component, but the response over land is weak and noisy (Figure 4.2l). This suggests that warm

CA margin SST induces a local thermodynamic precipitation response that is confined to the eastern Pacific [30, 2]. Over the SWUS, however, precipitation during MHWs is mainly induced by the circulation. This contrasts the decomposition of equilibrium mean precipitation, in which the thermodynamic component is not negligible (Figure 4.2g-i).

The thermodynamic contribution is much smaller than the circulation contribution across most experiments and models, indicating that precipitation during MHWs is dynamically-induced (Figure 4.3f-j). The circulation contribution is positive in the SWUS in all models except CCSM3, while the sign of the thermodynamic response varies across models. A precursor to CESM1.0.4, CCSM3 is the oldest and lowest resolution model included in our analysis. Large and Danabasoglu (2006) note that, even in higher resolution versions of CCSM3, coastal mountains in North America are not well represented and poor resolution of coastlines leads to biases in clouds and winds. We therefore lean towards trusting the newer and higher resolution models of the CMIP5 and CMIP6 generations, which offer a better representation of the coastline and the topography of the Rocky Mountains and the Sierra Madre Occidental.

4.3 Thermodynamics Drive the Discrepancy in the Southwest US Precipitation Response to Warm California Margin Sea Surface Temperature

The circulation-induced SWUS precipitation response to warm CA margin SST is positive in both equilibrium and during MHWs. When Figure 4.1 is recreated using only the circulation component of equilibrium mean precipitation changes, the relationship between CA margins SST and SWUS precipitation in equilibrium is in closer agreement with the relationship during MHWs (Figure 4.1b). During MHWs, a $1\ \sigma$ increase in CA margin SST corresponds to a $0.16\ \sigma$ increase in SWUS precipitation, on average. Under equilibrium warming, the multimodel mean total SWUS precipitation anomaly decreases $0.03\ \sigma$ for each $1\ \sigma$ increase in CA margin SST, whereas the dynamic component increases $0.09\ \sigma$.

The discrepancy in the SWUS precipitation response to MHWs and equilibrium mean warming (Figure 4.1a) can therefore be attributed to the thermodynamic response associated with mean state warming (Figure 4.1c). The multimodel mean slope of the equilibrium thermodynamic precipitation component is $-0.12\ \sigma$ per 1σ increase in CA margin SST. The cross model spread in the circulation- and thermodynamic-driven precipitation response to mean warming is of the same order of magnitude, with models varying more in the thermodynamic response.

Chapter 5

Summary, Discussion, and Implications

5.1 Summary

We find that the SWUS precipitation response differs when warm CA margin SST is a signature of internal variability-driven MHW events versus mean state warming due to higher CO_2 forcing. When the CA margin is warm *within* a given mean state, (i.e., during MHWs) SWUS precipitation is enhanced. In contrast, as the CA margin warms *across* equilibrium mean climates, models disagree on the response of SWUS precipitation. We use constructed circulation analogs (CCA) to decompose these different SWUS precipitation responses to anomalous CA margin SST into the thermodynamic and dynamic components.

Changes in low-level circulation increase SWUS precipitation both during MHWs and in equilibrium, but through different processes. During MHWs, the increase in precipitation is related to a weakening of the North Pacific Subtropical High, which allows for southerly flow from the tropics into the Gulf of CA, potentially initiating NAM precipitation. The increase in SWUS precipitation in equilibrium, however, is associated with higher SLP over the western US, which drives onshore geostrophic moisture transport from the Pacific into the SWUS.

We attribute the discrepancy in the sign of the total SWUS precipitation change during MHWs and in equilibrium to differences in thermodynamics. The thermodynamic component of precipitation during MHWs is negligible. The MHWs in our study are internally generated extreme events within a given mean climate. Because there are no significant changes in the background temperature or moisture content, thermodynamic effects are small and localized. On the other hand, both dynamics and thermodynamics contribute significantly to the SWUS precipitation response in equilibrium because changes in CO_2 forcing shift the mean climate state relative to the control. Changes in thermodynamic processes such as the land-ocean temperature and moisture contrasts, atmospheric evaporative demand, tropospheric stability, and land feedbacks suppress SWUS pre-

cipitation in higher CO_2 climates [73, 20, 74]. Consequently, MHWs are poor response and process analogs for idealized equilibrium SWUS precipitation change.

5.2 Discussion

The discrepancy in subtropical hydroclimates projected by climate models and inferred from past warm climates remains an outstanding issue in climate science. Analogs have been proposed to reconcile this mismatch, however conflating different types of analogs or ignoring differences in timescale can further obfuscate the discrepancy rather than provide clarity. For example, similarities in external climate forcings between the MPWP and near-future climate do not guarantee that the processes driving SWUS precipitation are the same in both climates.

One hypothesis proposed to explain the discrepancy in SWUS aridity inferred from MPWP proxy records and from climate model projections posits that elevated warming of the CA margin in the MPWP drove more monsoonal precipitation. Fu et al. (2022) show that modifying MPWP SSTs to better match proxy-inferred CA margin warmth drives increased SWUS summertime precipitation through enhanced mean moisture convergence and increased moist static energy. Bhattacharya et al. (2022) examine this mechanism in the MPWP using the 2014 eastern Pacific MHW, which was associated with enhanced monsoonal precipitation. Proposing MHWs as an analog for SWUS precipitation in the MPWP assumes that the drivers of SWUS precipitation during MHWs are similar to those governing long-term climate change. We test this assumption by assessing the relationship between CA margin SST and SWUS precipitation across numerous MHWs to cleanly identify the driving processes in the noisy precipitation fields. Moreover, both Bhattacharya et al. (2022) and Fu et al. (2022) investigate the CA margin SST-SWUS precipitation mechanism in a version of the CESM model, whereas we analyze this mechanism across five models. The equilibrium mean SWUS precipitation response in CESM1.0.4 and CCSM3, both part of the CESM family, deviates from the other models, highlighting the importance of evaluating hydroclimate responses and their drivers across a range of models.

Consistent with Bhattacharya et al. (2022), we find that localized CA margin warming during MHWs enhances SWUS precipitation through changes in the NAM circulation. In equilibrium, however, the more spatially uniform warming of the eastern Pacific does not guarantee a wetter SWUS. This contrast indicates that the spatial pattern of SST anomalies, rather than their magnitude alone, plays an important role in shaping SWUS precipitation responses. The SST warming pattern produced by the idealized simulations differs from MPWP SST reconstructions, which instead feature enhanced warming along coastal upwelling regions compared to surrounding regions [75, 32]. Previous work argues that the SWUS hydroclimate is sensitive to the eastern Pacific subtropical/tropical SST gradient through its influence on tropical ascent and subtropical subsidence [30, 20]. Although we do not explicitly analyze the gradient here, it is an inherent feature of MHWs and in equilibrium. MHWs are characterized by warmer CA margin SST relative to the tropical Pacific, so the wetter SWUS during MHWs is therefore also associated with a reduced subtropical/tropical gradient. While Bhattacharya et al. (2022) argue that SWUS precipitation during MHWs is more sensitive to the gradient than to CA margin SST alone, we find that the positive relationship between SST and precipitation emerges when considering only the CA margin. As for equilibrium, the five models we examine disagree on how the gradient changes across equilibrated climates (not shown), which may contribute to the intermodel spread in SWUS precipitation responses. Furthermore, differences between the gradient simulated in these idealized experiments and that inferred for the MPWP may help explain discrepancies between proxy evidence for a wetter SWUS and model-simulated aridity. Tropical eastern Pacific SST under CO_2 and other forcing are currently intensely debated [76, 77], so we focus on CA margin SST anomalies instead of meridional gradients to avoid additional uncertainty.

In addition to the SST pattern, limitations of our study include boundary conditions that differ from the MPWP and coarse model resolution. Our idealized simulations do not incorporate the vegetation, ice sheets, or topography characteristic of the MPWP. In CESM models, Brennan et al. (2022) show that CO_2 forcing accounts for only half of CA margin warming in the Pliocene, and attribute the other half to changes in vegetation and ice sheets. Moreover, the relatively coarse

resolution of our models might limit their ability to reproduce the degree of CA margin warming suggested by MPWP proxies [75, 24] and capture topography-driven precipitation [78, 20].

Despite these limitations, the dynamic/thermodynamic precipitation partition identified from the CCA decomposition emerges robustly across most models, regardless of differences in resolution and cloud, rain, and land surface parameterizations. Our findings are also consistent with other decomposition approaches applied to future projections. Using atmospheric moisture budget decomposition, Byrne and O'Gorman (2015) show that similar thermodynamic and dynamic partitioning in the SWUS emerges in the annual mean by the end of the 21st century, and Seager et al. (2014) show that these responses emerge in the summer half-year by 2040. Using a three-timescale decomposition, Zappa et al. (2020) highlight that drying in the western US due to the direct effect of CO_2 (timescale of months) is offset by a dynamic increase in precipitation driven by much slower evolving SST patterns. The relative strength of these contributions may differ between mean climates. For example, wetter conditions in the SWUS could weaken thermodynamic drying through reduced land–atmosphere feedbacks, while differences in Pacific SST patterns may alter the degree of moisture divergence over subtropical land [79].

Another hypothesis for a wetter SWUS in the MPWP posits that so-called "permanent El Niño" conditions, characterized by a reduced zonal SST gradient, drove increased wintertime precipitation [25, 26, 28, 80]. Our analysis focuses on the JJAS seasonal mean, but it remains an open question whether pluvial conditions in the MPWP were dominated by summertime or wintertime precipitation changes. Terrestrial proxies that can distinguish precipitation seasonality may therefore lend insight into mechanisms that generated widespread lakes in the SWUS during the MPWP [80, 29]. We do not investigate the change in the zonal SST gradient in equilibrium, or its relationship to wintertime dynamics, and we leave this as a direction for future work.

5.3 Implications for the Past and Future

Our results demonstrate that MHWs are not reliable response or process analogs for SWUS precipitation in warmer idealized equilibrium climates. Although localized CA margin warming

during MHWs is associated with increased SWUS precipitation through changes in the NAM circulation, equilibrium warming produces a different balance between dynamic and thermodynamic processes. Oldeman et al. (2025a) note that there is no a priori reason to expect a single perfect analog for any given climate state, so compositing several partial analogs can be insightful. Considering forcing, response, and process analogs together can therefore offer a more comprehensive interpretation of past and future climates.

To place our results in the context of the MPWP, we synthesize the characteristics of SST and precipitation during MHWs and in equilibrium across experiments. The magnitude of CA margin SST warming in our abrupt8x simulations (5-9K) resembles the estimated warming in the MPWP. However, the CO_2 forcing in the abrupt8x is almost five times higher than the upper estimate of that inferred for the MPWP, which is instead closer to (and likely lower than) the forcing in the abrupt2x experiment [81]. We show that the degree of thermodynamic drying scales with CO_2 forcing, so that, relative to the preindustrial climate, the thermodynamic drying in abrupt8x is greater than that in abrupt2x. This scaling implies that the thermodynamic-induced drying during the MPWP was likely weaker than in higher-CO_2 equilibrium climates. Consequently, the dynamic increase in precipitation associated with strong localized CA margin warming (the MHW mechanism) may have dominated the regional precipitation response and overwhelmed drying due to thermodynamics, resulting in a wetter SWUS. In this context, our results align with the hypothesis that localized CA margin warming contributed to pluvial conditions in the SWUS in the MPWP. However, eastern boundary current MPWP SST reconstructions remain uncertain due to highly variable estimates of the magnitude of warming (> 6°C between closely located sites) as well as limited spatial coverage, hindering our ability to constrain the extent of exceptionally warm eastern basin SST [82, 31]. The sensitivity of the SWUS hydroclimate to CA margin warming highlights that reducing this uncertainty and better understanding the mechanisms driving eastern boundary current warming is essential for reconciling the proxy-model mismatch.

Can CA margin MHWs provide an analog for the processes driving SWUS precipitation in future mean states? While MHWs illuminate the dynamical mechanisms linking SST anomalies and

SWUS precipitation, the strong thermodynamic effect inherent to mean state warming prevents them from fully constraining future equilibrium hydroclimate changes. Recent work has argued that the mechanisms governing near-term subtropical hydroclimate changes differ from those that emerge once the climate system has fully adjusted because of slow ocean adjustment [43]. This distinction implies that the relative importance of dynamic and thermodynamic processes changes as SST warming evolves. Consistent with this, our results demonstrate that SWUS hydroclimate is sensitive to both the pattern of SST warming and the balance between dynamic and thermodynamic contributions. Consequently, the future SWUS hydroclimate depends on the degree of CO_2 forcing, the pattern of SST warming, and the associated mean thermodynamic state, none of which MHWs capture. Accurate projections of future SWUS precipitation therefore require models that realistically capture the pattern of eastern Pacific SST warming and the balance between dynamic and thermodynamic processes.

Bibliography

[1] Pr Sheppard, Ac Comrie, Gd Packin, K Angersbach, and Mk Hughes. The climate of the US Southwest. *Climate Research*, 21:219–238, 2002.

[2] Tripti Bhattacharya, Ran Feng, Christopher R Maupin, Sloan Coats, Peter R Brennan, and Elizabeth Carter. California margin temperatures modulate regional circulation and extreme summer precipitation in the desert Southwest. *Environmental Research Letters*, 18(10):104048, 2023.

[3] Christopher L. Castro, Thomas B. McKee, and Roger A. Pielke. The Relationship of the North American Monsoon to Tropical and North Pacific Sea Surface Temperatures as Revealed by Observational Analyses. *Journal of Climate*, 14(24):4449–4473, 2001.

[4] Chao He, Tim Li, and Wen Zhou. Drier North American Monsoon in Contrast to Asian–African Monsoon under Global Warming. *Journal of Climate*, 33(22):9801–9816, 2020.

[5] R. W. Higgins, K.C. Mo, and Y. Yao. Interannual variability of the u.s. summer precipitation regime with emphasis on the southwestern monsoon. *Journal of Climate*, 11:2582–2606, 1998.

[6] Yochanan Kushnir, Richard Seager, Mingfang Ting, Naomi Naik, and Jennifer Nakamura. Mechanisms of Tropical Atlantic SST Influence on North American Precipitation Variability*. *Journal of Climate*, 23(21):5610–5628, 2010.

[7] Daniel F. Schmidt and Kevin M. Grise. Impacts of Subtropical Highs on Summertime Precipitation in North America. *Journal of Geophysical Research: Atmospheres*, 124(21):11188–11204, 2019.

[8] F. Song, R. L. Leung, and L. Dong. Future changes in seasonality of the north pacific and north atlantic subtropical highs. *Geophysical Research Letters*, 45:11959–11968, 2018.

[9] J. Karanja, B. M. Svoma, J. Walter, and M. Georgescu. Southwest us winter precipitation variability: reviewing the role of oceanic teleconnections. *Environmental Research Letters*, 18, 2023.

[10] D. Kurtzman and B. R. Scanlon. El nin o–southern oscillation and pacific decadal oscillation impacts on precipitation in the southern and central united states: Evaluation of spatial distribution and predictions. *Water Resources Research*, 18, 2007.

[11] D. F. Schmidt and K. M. Grise. Drivers of twenty-first-century u.s. winter precipitation trends in cmip6 models: A storyline-based approach. *Journal of Climate*, 34:6875–6889, 2021.

[12] Daniel R. Cayan, Tapash Das, David W. Pierce, Tim P. Barnett, Mary Tyree, and Alexander Gershunov. Future dryness in the southwest US and the hydrology of the early 21st century drought. *Proceedings of the National Academy of Sciences*, 107(50):21271–21276, 2010.

[13] Kevin M. Grise. Atmospheric Circulation Constraints on 21st Century Seasonal Precipitation Storylines for the Southwestern United States. *Geophysical Research Letters*, 49(17):e2022GL099443, 2022.

[14] Shannon M. Jones and David S. Gutzler. Spatial and Seasonal Variations in Aridification across Southwest North America. *Journal of Climate*, 29(12):4637–4649, 2016.

[15] Richard Seager, David Neelin, Isla Simpson, Haibo Liu, Naomi Henderson, Tiffany Shaw, Yochanan Kushnir, Mingfang Ting, and Benjamin Cook. Dynamical and Thermodynamical Causes of Large-Scale Changes in the Hydrological Cycle over North America in Response to Global Warming*. *Journal of Climate*, 27(20):7921–7948, 2014.

[16] Wengui Liang and Minghua Zhang. Increasing Future Precipitation in the Southwestern US in the Summer and Its Contrasting Mechanism With Decreasing Precipitation in the Spring. *Geophysical Research Letters*, 49(2):e2021GL096283, 2022.

[17] B. I. Cook and R. Seager. The response of the North American Monsoon to increased greenhouse gas forcing. *Journal of Geophysical Research: Atmospheres*, 118(4):1690–1699, 2013.

[18] Manuel Hernandez and Liang Chen. Future Land Precipitation Changes Over the North American Monsoon Region Using CMIP5 and CMIP6 Simulations. *Journal of Geophysical Research: Atmospheres*, 127(9):e2021JD035911, 2022.

[19] A. Hoell, C. Funk, M. Barlow, and S. Shukla. Recent and possible future variations in the north american monsoon. In *The Monsoons and Climate Change*, pages 149–162. Springer, 2016.

[20] Salvatore Pascale, William R. Boos, Simona Bordoni, Thomas L. Delworth, Sarah B. Kapnick, Hiroyuki Murakami, Gabriel A. Vecchi, and Wei Zhang. Weakening of the North American monsoon with global warming. *Nature Climate Change*, 7(11):806–812, 2017.

[21] L. E. Barton, A. M. Oldeman, A. M. Haywood, J. C. Tindall, A. M. Dolan, D. J. Hill, A. von der Heydt, and M. L. J. Baatsen. An assessment of the pliocene as an analogue for our warmer future. *Global and Planetary Change*, 252, 2025.

[22] K. D. Burke, J. W. Williams, M. A. Chandler, A. M. Haywood, D. J. Lunt, and B. L. Otto-Bliesner. Pliocene and Eocene provide best analogs for near-future climates. *Proceedings of the National Academy of Sciences*, 115(52):13288–13293, 2018.

[23] Jessica E. Tierney, Christopher J. Poulsen, Isabel P. Montañez, Tripti Bhattacharya, Ran Feng, Heather L. Ford, Bärbel Hönisch, Gordon N. Inglis, Sierra V. Petersen, Navjit Sagoo, Clay R. Tabor, Kaustubh Thirumalai, Jiang Zhu, Natalie J. Burls, Gavin L. Foster, Yves Goddéris, Brian T. Huber, Linda C. Ivany, Sandra Kirtland Turner, Daniel J. Lunt, Jennifer C. McElwain, Benjamin J. W. Mills, Bette L. Otto-Bliesner, Andy Ridgwell, and Yi Ge Zhang. Past climates inform our future. *Science*, 370(6517):eaay3701, 2020.

[24] J. E. Tierney, J. King, M. B. Osman, J. T. Abell, N. J. Burls, E. Erfani, V. T. Cooper, and R. Feng. Pliocene warmth and patterns of climate change inferred from paleoclimate data assimilation. *AGU Advances*, 6, 2025.

[25] Daniel E. Ibarra, Jessica L. Oster, Matthew J. Winnick, Jeremy K. Caves Rugenstein, Michael P. Byrne, and C. Page Chamberlain. Warm and cold wet states in the western United States during the Pliocene–Pleistocene. *Geology*, 46(4):355–358, 2018.

[26] S. Menemenlis, S. M. White, D. E. Ibarra, and J. M. Lora. A proxy-model comparison for mid-pliocene warm period hydroclimate in the southwestern us. *Earth and Planetary Science Letters*, 596, 2022.

[27] U. Salzmann, A. M. Haywood, D. J. Lunt, P. J. Valdes, and D. J. Hill. A new global biome reconstruction and data-model comparison for the middle pliocene. *Global Ecology and Biogeography*, 17:432–447, 2008.

[28] P. Molnar and M. A. Cane. El niño's tropical climate and teleconnections as a blueprint for pre-ice age climates. *Paleoceanography*, 17, 2002.

[29] M. J. Winnick, J. M. Welker, and C. P. Chamberlain. Stable isotopic evidence of El Niño-like atmospheric circulation in the Pliocene western United States. *Climate of the Past*, 9(2):903–912, 2013.

[30] Tripti Bhattacharya, Ran Feng, Jessica E. Tierney, Claire Rubbelke, Natalie Burls, Scott Knapp, and Minmin Fu. Expansion and Intensification of the North American Monsoon During the Pliocene. *AGU Advances*, 3(6):e2022AV000757, 2022.

[31] Minmin Fu, Mark A. Cane, Peter Molnar, and Eli Tziperman. Warmer Pliocene Upwelling Site SST Leads to Wetter Subtropical Coastal Areas: A Positive Feedback on SST. *Paleoceanography and Paleoclimatology*, 37(2):e2021PA004357, 2022.

[32] Petra S. Dekens, Ana Christina Ravelo, and Matthew D. McCarthy. Warm upwelling regions in the Pliocene warm period. *Paleoceanography*, 22(3):2006PA001394, 2007.

[33] Harry J Dowsett and Marci M Robinson. Mid-Pliocene equatorial Pacific sea surface temperature reconstruction: a multi-proxy perspective. *Philosophical Transactions of the Royal Society A: Mathematical, Physical and Engineering Sciences*, 367(1886):109–125, 2009.

[34] Martin Beniston. The 2003 heat wave in Europe: A shape of things to come? An analysis based on Swiss climatological data and model simulations. *Geophysical Research Letters*, 31(2):2003GL018857, 2004.

[35] Jeffrey Q. Chambers, Adriano José Nogueira Lima, Gilberto Pastorello, Bruno Oliva Gimenez, Lin Meng, Lee A. Dyer, Yanlei Feng, Cristina Santos Da Silva, Regison Costa De Oliveira, Anna Weber, Charlie Koven, Robinson Negrón-Juárez, Gustavo C. Spanner, Tatiana D. Gaui, Clarissa G. Fontes, Alessandro C. De Araújo, Nate McDowell, Ruby Leung, Daniel Magnabosco Marra, Jeffrey Warren, Daisy Celestina Souza, Cynthia Wright, Kolby Jardine, Marcos Longo, Chonggang Xu, Paul V. A. Fine, Rosie A. Fisher, Javier Tomasella, Joaquim Dos Santos, and Niro Higuchi. Hot droughts in the Amazon provide a window to a future hypertropical climate. *Nature*, 649(8099):1190–1196, January 2026.

[36] Claire B. Rubbelke, Tripti Bhattacharya, Ran Feng, Natalie J. Burls, Scott Knapp, and Erin L. McClymont. Plio-Pleistocene Southwest African Hydroclimate Modulated by Benguela and Indian Ocean Temperatures. *Geophysical Research Letters*, 50(19):e2023GL103003, 2023.

[37] Nicholas A. Bond, Meghan F. Cronin, Howard Freeland, and Nathan Mantua. Causes and impacts of the 2014 warm anomaly in the NE Pacific. *Geophysical Research Letters*, 42(9):3414–3420, 2015.

[38] Huan-Huan Chen, Yuntao Wang, Peng Xiu, Yi Yu, Wentao Ma, and Fei Chai. Combined oceanic and atmospheric forcing of the 2013/14 marine heatwave in the northeast Pacific. *npj Climate and Atmospheric Science*, 6(1):3, 2023.

[39] Emanuele Di Lorenzo and Nathan Mantua. Multi-year persistence of the 2014/15 North Pacific marine heatwave. *Nature Climate Change*, 6(11):1042–1047, 2016.

[40] Antonietta Capotondi, Regina R. Rodrigues, Alex Sen Gupta, Jessica A. Benthuysen, Clara Deser, Thomas L. Frölicher, Nicole S. Lovenduski, Dillon J. Amaya, Natacha Le Grix, Tongtong Xu, Juliet Hermes, Neil J. Holbrook, Cristian Martinez-Villalobos, Simona Masina,

Mathew Koll Roxy, Amandine Schaeffer, Robert W. Schlegel, Kathryn E. Smith, and Chunzai Wang. A global overview of marine heatwaves in a changing climate. *Communications Earth & Environment*, 5(1):701, 2024.

[41] Clara Deser, Adam S. Phillips, Michael. A. Alexander, Dillon J. Amaya, Antonietta Capotondi, Michael G. Jacox, and James D. Scott. Future Changes in the Intensity and Duration of Marine Heat and Cold Waves: Insights from Coupled Model Initial-Condition Large Ensembles. *Journal of Climate*, 37(6):1877–1902, 2024.

[42] E. C. J. Oliver, J. A. Benthuysen, S. Darmaraki, M. G. Donat, A. J. Hobday, N. J. Holbrook, R. W. Schlegel, and A. Sen Gupta. Marine heatwaves. *Annual Review of Marine Science*, 13:313–342, 2021.

[43] G. Zappa, P. Ceppi, and T. G. Shepard. Time-evolving sea-surface warming patterns modulate the climate change response of subtropical precipitation over land. *Proceedings of the National Academy of Sciences*, 117(9):4539–4545, 2020.

[44] Maria A. A. Rugenstein, Jonah Bloch-Johnson, Ayako Abe-Ouchi, Timothy Andrews, Urs Beyerle, Long Cao, Tejas Chadha, Gokhan Danabasoglu, Jean-Louis Dufresne, Lei Duan, Marie-Alice Foujols, Thomas L. Froelicher, Olivier Geoffroy, Jonathan M. Gregory, Reto Knutti, Chao Li, Alice Marzocchi, Thorsten Mauritsen, Matthew B. Menary, Elisabeth J. Moyer, Larissa S. Nazarenko, David J. Paynter, David Saint-Martin, Gavin A. Schmidt, Akitomo Yamamoto, and Shi Yang. Longrunmip: Motivation and design for a large collection of millennial-length aogcm simulations. *Bulletin of the American Meteorological Society*, 100(12):2551–2570, 2019.

[45] Gokhan Danabasoglu, Susan C. Bates, Bruce P. Briegleb, Steven R. Jayne, Markus Jochum, William G. Large, Synte Peacock, and Steve G. Yeager. The CCSM4 Ocean Component. *Journal of Climate*, 25(5):1361–1389, 2012.

[46] Peter R. Gent, Gokhan Danabasoglu, Leo J. Donner, Marika M. Holland, Elizabeth C. Hunke, Steve R. Jayne, David M. Lawrence, Richard B. Neale, Philip J. Rasch, Mariana Vertenstein, Patrick H. Worley, Zong-Liang Yang, and Minghua Zhang. The Community Climate System Model Version 4. *Journal of Climate*, 24(19):4973–4991, 2011.

[47] Maria A. A. Rugenstein, Jan Sedláček, and Reto Knutti. Nonlinearities in patterns of long-term ocean warming. *Geophysical Research Letters*, 43(7):3380–3388, 2016.

[48] Gokhan Danabasoglu and Peter R. Gent. Equilibrium Climate Sensitivity: Is It Accurate to Use a Slab Ocean Model? *Journal of Climate*, 22(9):2494–2499, 2009.

[49] S. G. Yeager, C. A. Shields, W. G. Large, and J. J. Hack. The low-resolution ccsm3. *Journal of Climate*, 19:2545–2566, 2006.

[50] Thorsten Mauritsen, Jürgen Bader, Tobias Becker, Jörg Behrens, Matthias Bittner, Renate Brokopf, Victor Brovkin, Martin Claussen, Traute Crueger, Monika Esch, Irina Fast, Stephanie Fiedler, Dagmar Fläschner, Veronika Gayler, Marco Giorgetta, Daniel S. Goll, Helmuth Haak, Stefan Hagemann, Christopher Hedemann, Cathy Hohenegger, Tatiana Ilyina, Thomas Jahns, Diego Jimenéz-de-la-Cuesta, Johann Jungclaus, Thomas Kleinen, Silvia Kloster, Daniela Kracher, Stefan Kinne, Deike Kleberg, Gitta Lasslop, Luis Kornblueh, Jochem Marotzke, Daniela Matei, Katharina Meraner, Uwe Mikolajewicz, Kameswarrao Modali, Benjamin Möbis, Wolfgang A. Müller, Julia E. M. S. Nabel, Christine C. W. Nam, Dirk Notz, Sarah-Sylvia Nyawira, Hanna Paulsen, Karsten Peters, Robert Pincus, Holger Pohlmann, Julia Pongratz, Max Popp, Thomas Jürgen Raddatz, Sebastian Rast, Rene Redler, Christian H. Reick, Tim Rohrschneider, Vera Schemann, Hauke Schmidt, Reiner Schnur, Uwe Schulzweida, Katharina D. Six, Lukas Stein, Irene Stemmler, Bjorn Stevens, Jin-Song Von Storch, Fangxing Tian, Aiko Voigt, Philipp Vrese, Karl-Hermann Wieners, Stiig Wilkenskjeld, Alexander Winkler, and Erich Roeckner. Developments in the MPI-M Earth System Model version 1.2 (MPI-ESM1.2) and Its Response to Increasing CO_2. *Journal of Advances in Modeling Earth Systems*, (4):998–1038, 2019.

[51] Tim Rohrschneider, Bjorn Stevens, and Thorsten Mauritsen. On simple representations of the climate response to external radiative forcing. *Climate Dynamics*, 53(5-6):3131–3145, 2019.

[52] Long Cao, Lei Duan, Govindasamy Bala, and Ken Caldeira. Simulated long-term climate response to idealized solar geoengineering. *Geophysical Research Letters*, 43(5):2209–2217, 2016.

[53] Peter M. Cox, Richard A. Betts, Chris D. Jones, Steven A. Spall, and Ian J. Totterdell. Acceleration of global warming due to carbon-cycle feedbacks in a coupled climate model. *Nature*, 408(6809):184–187, 2000.

[54] A. Voldoire, D. Saint-Martin, S. Sénési, B. Decharme, A. Alias, M. Chevallier, J. Colin, J.-F. Guérémy, M. Michou, M.-P. Moine, P. Nabat, R. Roehrig, D. Salas Y Mélia, R. Séférian, S. Valcke, I. Beau, S. Belamari, S. Berthet, C. Cassou, J. Cattiaux, J. Deshayes, H. Douville, C. Ethé, L. Franchistéguy, O. Geoffroy, C. Lévy, G. Madec, Y. Meurdesoif, R. Msadek, A. Ribes, E. Sanchez-Gomez, L. Terray, and R. Waldman. Evaluation of CMIP6 DECK Experiments With CNRM-CM6-1. *Journal of Advances in Modeling Earth Systems*, 11(7):2177–2213, 2019.

[55] N. J. Holbrook, H. A. Scannell, A. Sen Gupta, J. A. Benthuysen, M. Feng, E. C. J. Oliver, L. V. Alexander, M. T. Burrows, M. G. Donat, P. J. Hobday, A. J.and Moore, S. E. Perkins-Kirkpatrick, D. A. Smale, S. C. Straub, and T. Wernberg. A global assessment of marine heatwaves and their drivers. *Nature Communications*, 10(2624), 2019.

[56] Clara Deser, Laurent Terray, and Adam S. Phillips. Forced and Internal Components of Winter Air Temperature Trends over North America during the past 50 Years: Mechanisms and Implications*. *Journal of Climate*, 29(6):2237–2258, 2016.

[57] F. Lehner, C. Deser, I. R. Simpson, and L. Terray. Attributing the u.s. southwest's recent shift into drier conditions. *Geophysical Research Letters*, 45:6251–6261, 2018.

[58] M. J. Rodwell and B. J. Hoskins. Subtropical anticyclones and summer monsoons. *Journal of Climate*, 14:3192–3211, 2000.

[59] Nikolaos Christidis and Peter A. Stott. Changes in the geopotential height at 500 hPa under the influence of external climatic forcings. *Geophysical Research Letters*, 42(24), 2015.

[60] Salvatore Pascale, Sarah B. Kapnick, Simona Bordoni, and Thomas L. Delworth. The Influence of CO_2 Forcing on North American Monsoon Moisture Surges. *Journal of Climate*, 31(19):7949–7968, 2018.

[61] Ehsan Erfani and David Mitchell. A partial mechanistic understanding of the North American monsoon. *Journal of Geophysical Research: Atmospheres*, 119(23), 2014.

[62] David L. Mitchell, Dorothea Ivanova, Robert Rabin, Timothy J. Brown, and Kelly Redmond. Gulf of California Sea Surface Temperatures and the North American Monsoon: Mechanistic Implications from Observations. *Journal of Climate*, 15(17):2261–2281, 2002.

[63] Matthew C. Brewer and Clifford F. Mass. Projected Changes in Western U.S. Large-Scale Summer Synoptic Circulations and Variability in CMIP5 Models. *Journal of Climate*, 29(16):5965–5978, 2016.

[64] David K. Adams and Andrew C. Comrie. The North American Monsoon. *Bulletin of the American Meteorological Society*, 78(10):2197–2213, 1997.

[65] C Roberto Mechoso, Andrew W Robertson, Chester F Ropelewski, and Alice M Grimm. The American Monsoon Systems. 2004.

[66] Isla R. Simpson, Karen A. McKinnon, Daniel Kennedy, David M. Lawrence, Flavio Lehner, and Richard Seager. Observed humidity trends in dry regions contradict climate models. *Proceedings of the National Academy of Sciences*, 121(1):e2302480120, 2024.

[67] A. Park Williams, Edward R. Cook, Jason E. Smerdon, Benhjamin I. Cook, T. Abatzoglou, John, Kasey Bolles, Seung H. Baek, Andrew M. Badger, and Ben Livneh. Large contri-

bution from anthropogenic warming to an emerging north american megadrought. *Science*, 368:314–318, 2020.

[68] Sonali Shukla McDermid, Benjamin I. Cook, Martin G. De Kauwe, Justin Mankin, Jason E. Smerdon, A. Park Williams, Richard Seager, Michael J. Puma, Igor Aleinov, Maxwell Kelley, and Larissa Nazarenko. Disentangling the Regional Climate Impacts of Competing Vegetation Responses to Elevated Atmospheric CO_2. *Journal of Geophysical Research: Atmospheres*, 126(5):e2020JD034108, 2021.

[69] Samuel Villarreal, Rodrigo Vargas, Enrico A. Yepez, Jose S. Acosta, Angel Castro, Martin Escoto-Rodriguez, Eulogio Lopez, Juan Martínez-Osuna, Julio C. Rodriguez, Stephen V. Smith, Enrique R. Vivoni, and Christopher J. Watts. Contrasting precipitation seasonality influences evapotranspiration dynamics in water-limited shrublands. *Journal of Geophysical Research: Biogeosciences*, 121(2):494–508, 2016.

[70] Thuy Trang Vo, Leiqiu Hu, Lulin Xue, and Sisi Chen. Trends in Cloud Covers across CONUS (1980–2020). *Journal of Climate*, 38:5371–5390, 2025.

[71] Xue-Yan Zhang, Jiming Jin, Xubin Zeng, Charles P. Hawkins, Antônio A. M. Neto, and Guo-Yue Niu. The Compensatory CO_2 Fertilization and Stomatal Closure Effects on Runoff Projection From 2016–2099 in the Western United States. *Water Resources Research*, 58(1):e2021WR030046, 2022.

[72] Michael P. Byrne and Paul A. O'Gorman. Trends in continental temperature and humidity directly linked to ocean warming. *Proceedings of the National Academy of Sciences*, 115(19):4863–4868, 2018.

[73] Michael P. Byrne and Paul A. O'Gorman. The Response of Precipitation Minus Evapotranspiration to Climate Warming: Why the "Wet-Get-Wetter, Dry-Get-Drier" Scaling Does Not Hold over Land*. *Journal of Climate*, 28(20):8078–8092, 2015.

[74] A. Park Williams, Edward R. Cook, Jason E. Smerdon, Benjamin I. Cook, John T. Abatzoglou, Kasey Bolles, Seung H. Baek, Andrew M. Badger, and Ben Livneh. Large contribution from anthropogenic warming to an emerging North American megadrought. *Science*, 368(6488):314–318, 2020.

[75] P. R. Brennan, T. Bhattacharya, R. Feng, J. E. Tierney, and E. M. Jorgensen. Patterns and mechanisms of northeast pacific temperature response to pliocene boundary conditions. *Paleoceanography and Paleoclimatology*, 37:e2021PA004370, 2022.

[76] Ulla K. Heede, Alexey V. Fedorov, and Natalie J. Burls. Time scales and mechanisms for the tropical pacific response to global warming: A tug of war between the ocean thermostat and weaker walker. *Journal of Climate*, 33:6101–6118, 2020.

[77] Yen-Ting Hwang, Shang-Ping Xie, Po-Ju Chen, Hung-Yi Tseng, and Clara Deser. Contribution of anthropogenic aerosols to persistent la niña-like conditions in the early 21st century. *Proceedings of the National Academy of Sciences*, 121(5):e2315124121, 2024.

[78] W. R. Boos and S. Pascale. Mechanical forcing of the north american monsoon by orography. *Nature*, 599:611–615, 2021.

[79] N. J. Burls and A. V. Fedorov. Wetter subtropics in a warmer world: Contrasting past and future hydrological cycles. *Proceedings of the National Academy of Sciences*, 6(49):12888–12893, 2017.

[80] S. Spaur, D. J. Koning, M. Heizler, S. Aby, G. Williamson, J. R. Knott, R. P. Acosta, and J. K. C. Rugenstein. The hydroclimate and environmental response to middle miocene warming in the southwestern usa: Stable isotope evidence. *Paleoceanography and Paleoclimatology*, 40, 2025.

[81] Bärbel Hönisch, Dana L. Royer, Daniel O. Breecker, Pratigya J. Polissar, Gabriel J. Bowen, Michael J. Henehan, et al. Toward a cenozoic history of atmospheric co2. *Science*, 382(6675):eadi5177, 2023.

[82] J. D. Annan, J. C. Hargreaves, T. Mauritsen, E. McClymont, and S. L Ho. Can we reliably reconstruct the mid-pliocene warm period with sparse data and uncertain models? *Climate of the Past*, 20:1989–1999, 2024.

[83] Russell L. Horowitz, Karen A. McKinnon, and Isla R. Simpson. Circulation and Soil Moisture Contributions to Heatwaves in the United States. *Journal of Climate*, 35(24):8031–8048, 2022.

[84] Laurent Terray. A dynamical adjustment perspective on extreme event attribution. *Weather and Climate Dynamics*, 2(4):971–989, 2021.

Appendix A

Constructed Circulation Analogs

Here we explain how we apply the CCA method to the equilibrium mean and MHW composite in detail.

A.1 Applied to Equilibrium

For each model, experiment, and variable of interest (here we are using JJAS SLP and precipitation), we subtract the control equilibrium mean to obtain absolute SLP and precipitation anomalies relative to the control. We aim to recreate the equilibrium mean SLP anomaly, which averages out high frequency internal circulation variability and represents the low level summertime circulation anomaly relative to the control climate. The process is shown in Figure A.1 and is as follows for the equilibrium mean scenario:

1. Obtain the spatial equilibrium SLP anomaly map from 8.75°S-51.25°N and 68.75°W-178.75°W (target SLP). We utilize a large geographic domain for SLP following Terray (2021), who notes that the circulation-driven response of a given variable is meaningful only over a domain within and smaller than the SLP domain. The analog library is the control SLP and precipitation anomalies for each model and contains N_t summers

2. Compute the Euclidean distance between the target SLP and each summer in the analog library. We obtain the N_a summers in the analog library in which the SLP most closely resembles (i.e., has the lowest distance to) the target SLP

3. Repeat the following N_r times:

    - Randomly subsample N_s of the N_a analogs without replacement
    - Calculate the regression coefficients from a multilinear regression of the target SLP map (predictand) onto the N_s SLP analog library maps (predictors)

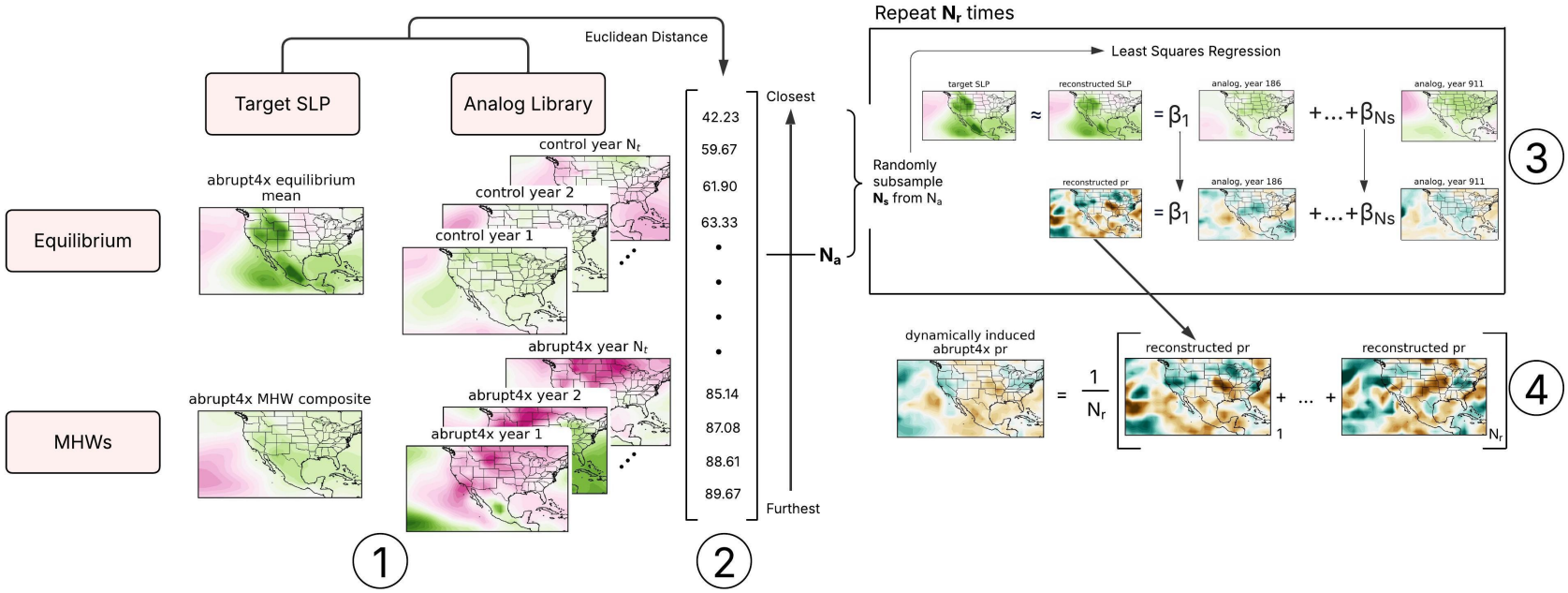

Figure A.1: The constructed circulation analog method

- Linearly combine the N_s analogs by weighting each by the regression coefficient to obtain a reconstruction of the target SLP
- Apply the same weights to the corresponding precipitation anomaly maps in the analog library to obtain the precipitation field associated with the SLP reconstruction

4. Average the N_r reconstructions to get the final best estimate of the target SLP and the precipitation associated with this pattern

The precipitation associated with the SLP reconstruction is the dynamically-induced component of the total response and is a result of only the forced change in SLP because the analogs do not contain thermodynamic forcing. This differs from other applications of CCA in which the dynamic component is a result of unforced internal variability [83], observed circulation patterns [57, 84], or further decomposed into the internal and forced circulation response [56]. By reconstructing the 200-year long equilibrium mean SLP from the control, we are creating an analog for the forced circulation change from the relationships present in internal circulation variability. We subtract the dynamic component of SLP and precipitation from the total equilibrium anomaly to get the residual. In the case of the target SLP, the residual reflects how well we are able to linearly construct the target SLP from the analog library.

For the equilibrium application, we set N_a = 150, N_s = 70, and N_r = 100. N_t is the total number of years available in the control, which is 1000 years for most models. For N_a, N_r, and N_s we choose the value where the root mean square error (RMSE) between the SLP reconstruction and the SLP target does not change appreciably. Our results are relatively insensitive to the choice of N_a and N_r, while N_s is the most sensitive parameter (Figure A.2, left).

A.2 Applied to Marine Heatwaves

We reconstruct the MHW SLP anomaly from the non-MHW summers in each respective experiment. For each model, we detrend as described in section 2.3 and utilize the same domain as in the equilibrium scenario. We then remove all 80 MHWs from each experiment. We treat

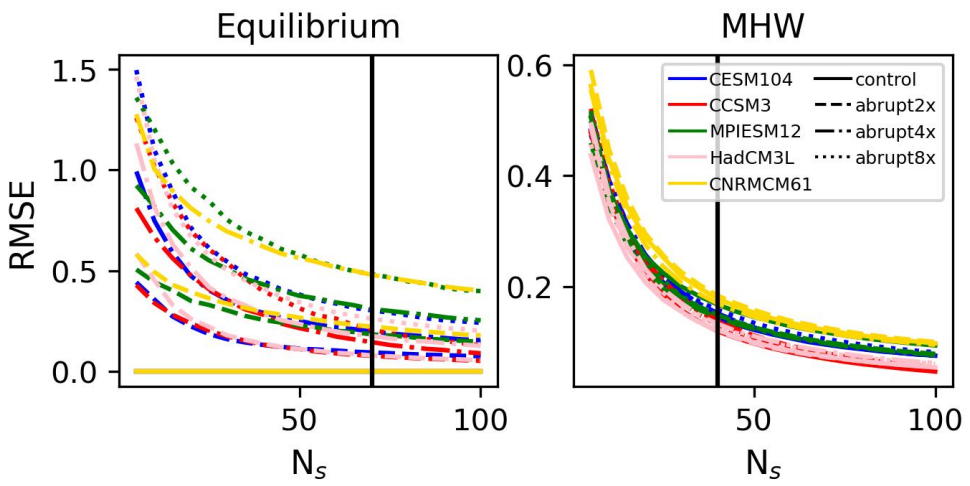

Figure A.2: Root mean square error between the constructed and target sea level pressure as a function of N_s for the equilibrium (left) and marine heatwave (right) sea level pressure anomaly. Vertical black lines are the values of N_s used in this analysis.

each MHW as a separate target SLP and reconstruct the SLP anomaly from the pool of remaining years (analog library). We then perform steps 2-4 as outlined above. We repeat the process for each of the remaining MHWs, and lastly average each best estimate together to get the final reconstruction. As before, we subtract the linearly reconstructed SLP and precipitation maps from the total anomaly to get the residual. This method is a more typical application of CCA because the dynamic component is constructed from the internal atmospheric variability that characterizes each mean climate state. For the MHW application we use N_a = 150, N_s = 40, and N_r = 100. N_t is 720 years for most experiments because we remove the first 200 years following the forcing before detrending (see section 2.3), then remove the MHW years. Our results are insensitive to the choice of N_a and N_r, but not N_s (Figure A.2, right)

Appendix B

Supplementary Figures

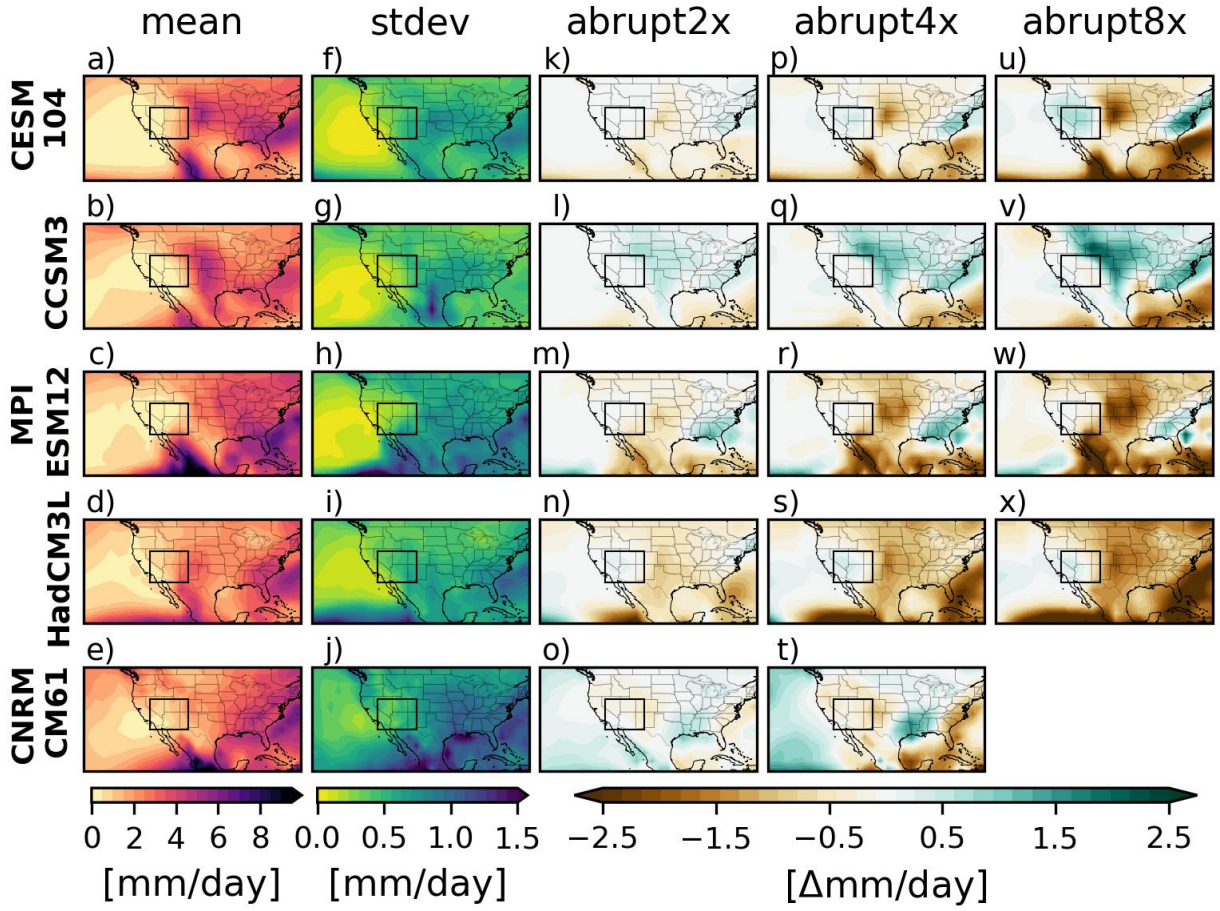

Figure B.1: Control equilibrium mean summer precipitation (a-e) and standard deviation (f-j). abrupt2x (k-o), abrupt4x (p-t), and abrupt8x (u-x) anomalies of precipitation with respect to the control. The box indicates the Southwest region, 103.75-118.75°W and 31.25-41.25°N.

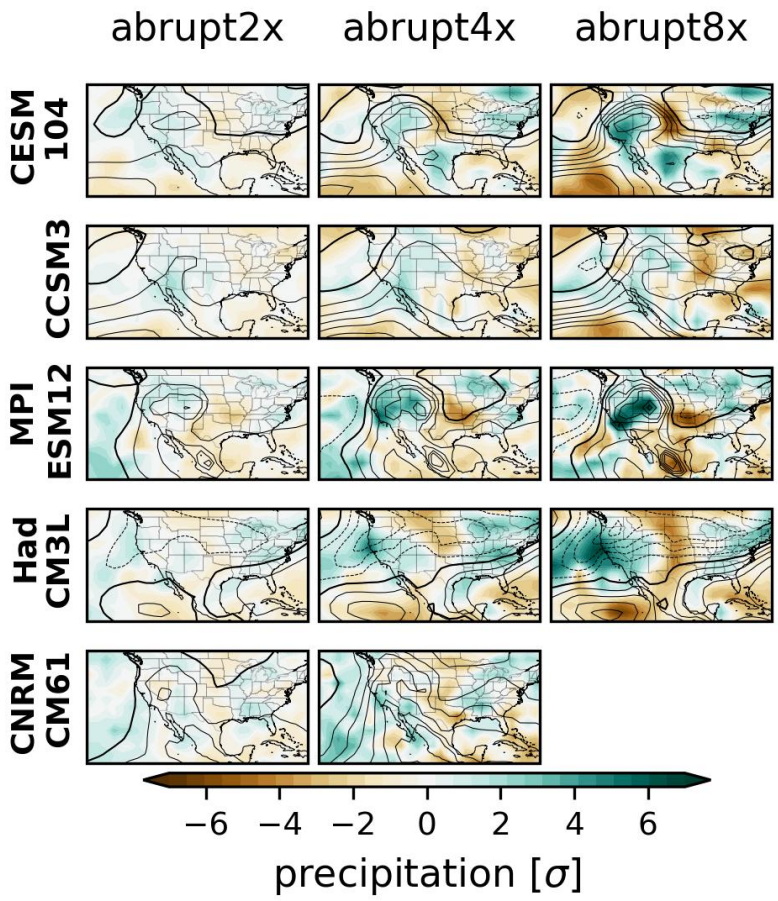

Figure B.2: Dynamic component of the equilibrium mean precipitation anomaly (colors) and the reconstructed sea level pressure anomaly (black contours, 1 standard deviation increments, thick lines represent no change and thin solid and dashed lines represent an increase and decrease in sea level pressure, respectively).

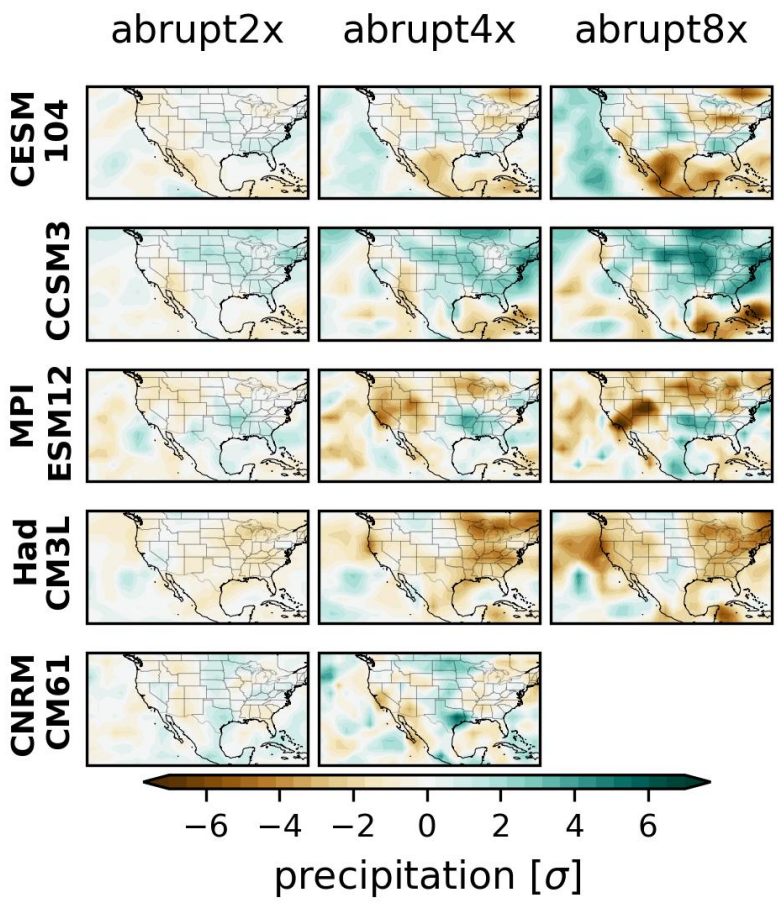

Figure B.3: Thermodynamic component of the equilibrium mean precipitation anomaly.

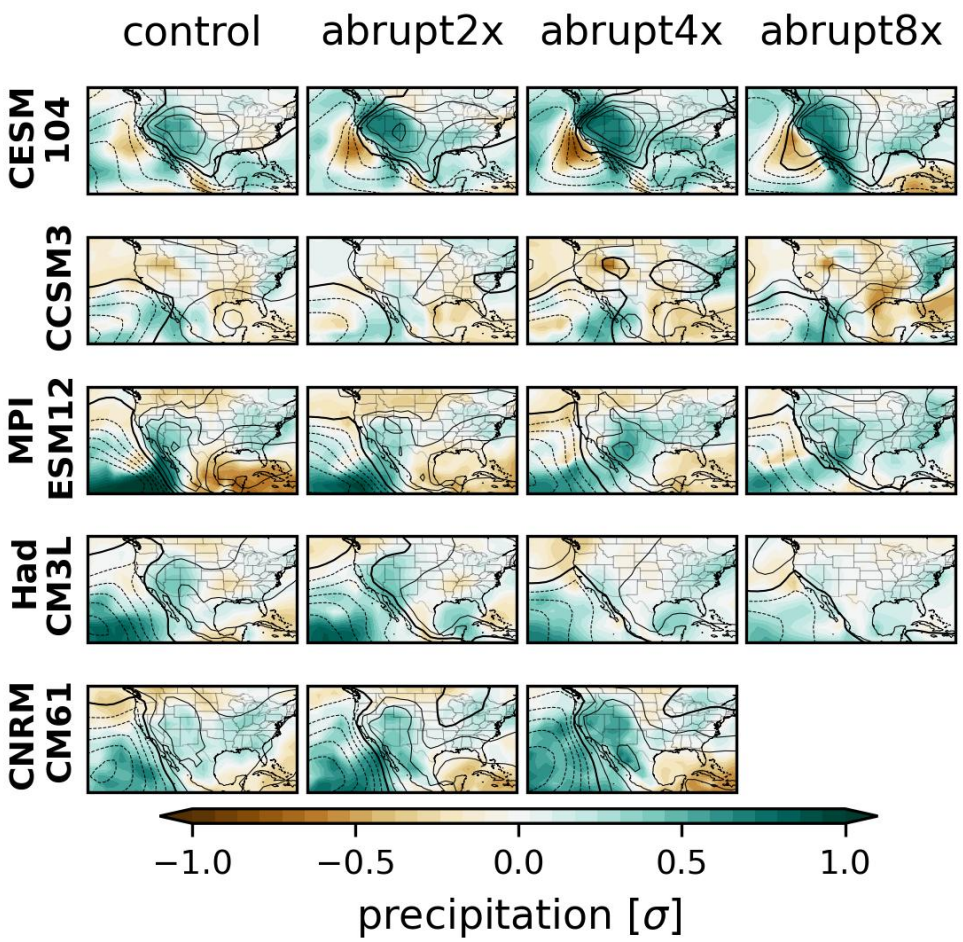

Figure B.4: Dynamic component of the precipitation anomaly (colors) and the reconstructed sea level pressure anomaly (black contours, increments of 0.2 standard deviations, thick lines represent no change and thin solid and dashed lines represent an increase and decrease in sea level pressure, respectively) during marine heatwaves.

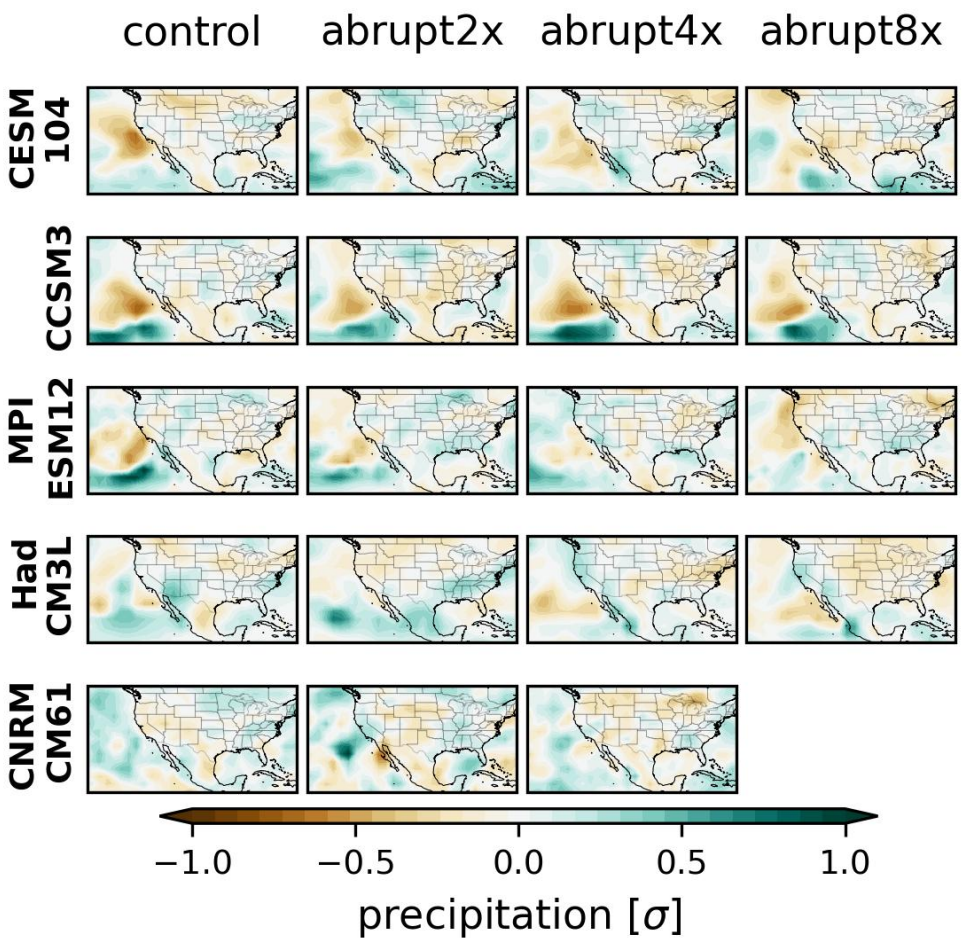

Figure B.5: Thermodynamic component of the precipitation anomaly during marine heatwaves.